Phosphorylation of the Type VI secretion system sheath controls *Francisella* virulence

Jason Ziveri[1], Cerina Chhuon[2], Anne Jamet[1], Guénolé Prigent[1], Fabiola Tros[1], Monique Barel[1], Claire Lays[4], Thomas Henry[4], Nicholas H Keep[3], Ida Chiara Guerrera[2]*, Alain Charbit[1]*

[1] Université Paris Descartes, Sorbonne Paris Cité, Bâtiment Leriche, Paris, INSERM U1151 - CNRS UMR 8253, Institut Necker-Enfants Malades. Team 11: Pathogenesis of Systemic Infections, Paris, France

[2] Plateforme protéomique 3P5-Necker, Université Paris Descartes - Structure Fédérative de Recherche Necker, INSERM US24/CNRS UMS3633, Paris 75014, France

[3] Crystallography, Institute for Structural and Molecular Biology, Department of Biological Sciences Birkbeck, University of London, United Kingdom

[4] CIRI, Centre International de Recherche en Infectiologie, Université Lyon, Inserm, U1111, University Claude Bernard Lyon 1, CNRS, UMR5308, École Normale Supérieure de Lyon, Labex Ecofect, Eco-evolutionary dynamics of infectious diseases, F-69007, LYON, France

Running title: Phosphorylation of IglB is critical for *Francisella* sheath assembly

Keywords: Type 6 secretion system, Phosphoproteome, *Francisella tularensis*, IglB.

Bâtiment Leriche. 14 Rue Maria Helena Vieira Da Silva CS 61431 - 75993 PARIS – FRANCE

*Corresponding authors: Ida Chiara Guerrera, Alain Charbit.

e-mail: alain.charbit@inserm.fr; chiara.guerrera@inserm.fr

Tel: 33 1 – 72 60 65 11 — Fax: 33 1 - 72 60 65 13

Abstract

Many Gram-negative bacteria use type VI secretion systems (T6SS) to translocate effector proteins into eukaryotic or prokaryotic cells. *Francisella* possesses a non-canonical T6SS encoded on the *Francisella* pathogenicity island (FPI) that is essential for efficient phagosomal escape and access to the cytosol of infected host cells. Using a global and site-specific phosphoproteomic analysis of *Francisella*, we identified a unique phosphorylation site on tyrosine 139 of IglB, the TssC homologue and a key component of the T6SS contractile sheath. Phosphorylated IglB was exclusively found in the non-oligomerized form of the protein, suggesting that sheath assembly requires IglB dephosphorylation. All the different amino acid substitutions at site 139 of IglB all impaired sheath assembly. The data presented suggest that the phosphorylation status of IglB plays a critical role in T6SS activity and, hence, *Francisella* pathogenicity. We propose that this post-translational modification of the sheath may constitute a previously unrecognized mechanism to modulate the dynamics of assembly-disassembly of the T6SS.

Author summary

Francisella possesses a non-canonical T6SS that is essential for efficient phagosomal escape and access to the cytosol of infected host cells. Using a global and site-specific phosphoproteomic analysis of *Francisella* we identified here a unique phosphorylation site on IglB, the TssC homologue and a key component of the T6SS contractile sheath. Our data suggest that the phosphorylation status of IglB plays a critical role in the assembly of a functional T6SS. This post-translational modification of the sheath may constitute a previously unrecognized mechanism to modulate the dynamics of assembly-disassembly of the T6SS.

Introduction

Francisella tularensis is the causative agent of the zoonotic disease tularemia (1-4). This facultative intracellular pathogen is able to infect a variety of different cell types but, *in vivo*, is thought to replicate and disseminate mainly in phagocytes (5). The four major subspecies (subsp) of *F. tularensis* currently listed are the subsps: *tularensis*, *holarctica, mediasiatica* and *novicida* (the latter is also called *F. novicida*). These subspecies differ in their virulence and geographical origin (6) but all cause a fulminant disease in mice that is similar to tularemia in humans (7). Although *F. novicida* is rarely pathogenic in humans, its genome shares a high degree of nucleotide sequence conservation with the human pathogenic species and is thus widely used as a model to study highly virulent subspecies (8-10). The efficiency of *Francisella* systemic dissemination is tightly linked to its capacity to multiply in the cytosolic compartment of infected macrophages. The transcriptional and post-transcriptional regulatory processes, controlling phagosomal escape and cytosolic bacterial multiplication, have been already well-characterized (11-17). In contrast, the contribution of post-translational protein modifications (PTMs) has remained largely underestimated. For example, protein glycosylation has been only very recently identified in *Francisella* (18, 19) and the importance of protein phosphorylation in *Francisella* pathogenesis is still largely unknown (20), although it constitutes one of the most prevalent PTM involved in controlling protein activity.

Two major systems of protein phosphorylation exist in Gram-negative bacteria: i) two-component systems (TCSs), composed of a membrane-bound sensor kinase that auto-phosphorylates at a conserved histidine residue and a cognate response regulator that is phosphorylated at a conserved aspartate residue; and ii) serine/threonine or tyrosine protein kinases (Ser/Thr/Tyr-K) and their associated phosphatases (21-23 and references therein). In addition, many Gram-negative bacteria also possess a phospho-relay system, designated phosphoenol pyruvate:carbohydrate phosphotransferase system (or PTS), that is more

78 specifically devoted to sugar transport (24, 25 and references therein). *Francisella* genomes,
79 do not encode any PTS (26) but encode elements of two-component regulatory systems
80 (TCS). Whereas most *Francisella* strains possess only incomplete TCS pairs (27), *F.*
81 *novicida* has two complete and two incomplete TCS pairs (28, 29).
82
83 Our careful inspection of the *Francisella* genomes did not identify any gene encoding for a
84 putative serine/threonine-protein kinase or tyrosine kinase. In spite of this lack of canonical
85 kinases, we hypothesized that such post-translational protein modifications might occur in
86 *Francisella* and contribute to pathogenesis. By using state-of-the art mass spectrometry
87 analyses, we identified and quantified 82 peptides bearing phosphorylated residues in the
88 proteome of *F. novicida.* One peptide, corresponding to a phosphorylation of IglB on tyrosine
89 139 (Tyr139), particularly attracted our attention. Indeed, IglB is analogous to the TssC
90 protein in canonical T6SS and oligomerizes with IglA (TssB homologue) to form the
91 contractile sheath (30) of its type six secretion apparatus (T6SS).
92 T6SS have been described as contractile syringes used by bacterial species either to kill
93 neighboring bacteria competing for the same niche or to target eukaryotic cells upon
94 infection. Bioinformatic analyses have divided bacterial T6SS in three phylogenetically
95 distinct subtypes (designated T6SSi-iii) (31). Whereas most of the well-characterized T6SS
96 belong to the T6SSi (including in *P. areruginosa* and *V. cholerae*), *Francisella* is currently the
97 only bacterium to possess a T6SSii family member (32). *Francisella* T6SS has been shown,
98 thus far, to be exclusively involved in the intracellular life cycle of the pathogen. Phagosomal
99 escape occurs as early as 30 minutes post-infection (33) and critically depends on the T6SS
100 that is encoded by a 33 kb locus named *Francisella* pathogenicity island (FPI) (34-36, 37,
101 38). The FPI (**Supplementary Fig. 1**) also encodes a number of proteins of unknown
102 functions, some of which (such as IglF,PdpC or PdpD) have been proposed to be T6SS
103 effectors(9). Remarkably, the FPI does not encode any homologue of the unfoldase ClpV,
104 present in all the canonical T6SS, involved in the recycling of the contracted sheaths.
105 However, it has been recently shown that, in *F. novicida*, the general chaperone ClpB (39)

could fulfill ClpV function(8) by specifically colocalizing with the contracted sheath and promoting its disassembly. Of note, the FPI is duplicated in all the subspecies of *F. tularensis* except in *F. novicida*, in which it is present in a single copy.

Our current knowledge of the structure and functional assembly of the *Francisella* T6SSii are mainly based on recent cryo-electron microscopy data (30) and structural homologies with other members of the T6SSi. It has been proposed that the tube comprised of IglC subunits (Hcp homologue) that form hexameric rings, fits within the cavity of the IglA/IglB sheath (TssB/C in *Pseudomonas*, VipA/B in *Vibrio*). Contraction of the sheath results in the ejection of the Hcp tube, together with effector proteins located within the tube and on top of the tip of the tube (40). By analogy with other T6SS structural data, it has been suggested but not formally proven that, in *Francisella*, the sheath assembles on a preassembled IglC tube (30). This assumption awaits additional structural information on the different conformations of the *Francisella* T6SS (from fully elongated to fully contracted stages).

The data presented here reveal that the phosphorylation status of a single tyrosine residue of IglB is essential for the proper activity of the T6SS and, hence, *Francisella* pathogenicity. We propose that, upon infection, this post-translational mechanism may participate in the control of T6SS dynamics, for a rapid and reversible response to its different intracellular environments.

127 # Results

128

129 **The phosphoproteome of *Francisella***

130 We carried out a global and site-specific phosphoproteomic analysis of *F. novicida* (strain
131 U112), based on phosphopeptide enrichment and high-resolution LC-MS/MS determination
132 of whole cell lysates (see Methods). This analysis detected 82 phosphopeptides (68 with
133 high probability for site attribution). The majority of the phosphosites (53 out of 82) were
134 found on serine residues (S), while similar lower number of sites, 13 and 16, were found on
135 threonine (T) and tyrosine (Y), respectively (**Fig 1A and S1 and Tables**).

136

137 **Fig1. The phosphoproteome of *F. novicida***

138 (**A**) Distribution of phosphosites according to the modified amino acid (tyrosine,Y; threonine,
139 T and serine, S). (**B**) Logos of phosphopeptide amino acid sequences; (**C**) Histograms of the
140 most represented classes of protein. The values correspond to the number of proteins
141 bearing phosphosites in each category.

142

143 In order to highlight possible consensus sequences, we aligned the sequences of the
144 phosphoserine / threonine / tyrosine peptides. Although the number of peptides is perhaps
145 too low to be conclusive, we could observe the recurrence of some amino acids in specific
146 positions, like lysine (K) in position n-1 of phosphothreonines (pT) or apolar amino acids
147 valine and phenylalanine (V, F) in n-1 of phosphotyrosines (pY) (**Fig 1B**). These
148 phosphosites corresponded to 49 proteins, of which 13 presented multiple phosphorylation
149 sites. The 49 proteins belonged to various functional categories and the most represented
150 classes were carbohydrate metabolism, energy production and conversion and translation
151 (**Fig 1C**).

152 Remarkably, the two proteins that constitute the T6SS sheath(30, 41, 42) (IglA and IglB,
153 **S1 Fig**) appeared to bear a unique phosphorylation site (at Ser173 for IglA, and Tyr139 for
154 IglB). This somewhat unexpected observation prompted us to determine whether the
155 phosphorylated forms of the two proteins were incorporated into the sheath upon its
156 assembly. For this, we first monitored sheath formation using the procedure previously
157 described in (30). Briefly, lysates of wild-type *F. novicida,* grown in the presence of 5% KCl in
158 order to trigger sheath formation, were layered onto 15%-55% sucrose gradients (**Fig 2A**)
159 and the different fractions were tested by western blotting with anti-Igl (A,B or C) antibodies.
160 IglA and IglB were detected in all the fraction of the gradient, although with variable
161 intensities (**Fig 2B**). In contrast, IglC was only detected in the upper fractions of the gradient
162 (in the 15% and in part of the 35% fractions). The fractions sedimenting in equilibrium at 55%
163 sucrose and below (55% Optiprep, grey arrow, **Fig 2A**) were further dialyzed and used for
164 negative staining TEM imaging. Confirming earlier reports, we observed rod-shaped particles
165 of variable length in this fraction by electron microscopy, corresponding to assembled
166 sheath-like structures (**Fig 2A**). We then compared by mass spectrometry the fractions at the
167 bottom of the gradient (sucrose 55%-Optiprep 55% density zone) that contained these
168 sheath-like particles, to the fractions at the top of the gradient (15-35% sucrose density
169 zone), presumably containing non-polymerized forms of the IglA and IglB proteins (hereafter
170 called “heavy fraction”, H or “light fraction”, L, respectively). The mass spectrometry analysis
171 of the H and L fractions identified over 1,145 proteins (**S3 Table**). Of note, proteins
172 exclusively identified in the H fraction included several Type IV pili assembly proteins (fimT,
173 PilE, PilF) that might interact with the sheath. IglA and IglB were detected in both H and L
174 fractions. In order to estimate the proportion of the Igl proteins in the two fractions, we
175 calculated the ratio of the intensity of the protein, proportional to the amount of protein in the
176 fraction. Fully supporting the western blotting analyses, IglA and B were more abundant in
177 the L fraction than in the H fraction and only 2% of IglC was detected in the H fraction (**Fig**
178 **2C**).

179 As illustrated in **Fig 2D**, the peptide bearing the phosphorylated tyrosine residue (pY139)
180 of IglB was exclusively detected in the L fraction of the gradient, suggesting that only the
181 soluble forms of IglB are phosphorylated (**S3 Table**). Unmodified peptides containing Tyr139
182 were however detected in both H and L fractions, indicating that soluble IglB include both
183 phosphorylated and unphosphorylated forms of the protein. The phosphopeptide, bearing the
184 phosphorylated serine residue of IglA, identified in the whole cell lysate, was not detected in
185 either of the two samples analyzed. This lack of detection could be due either to an
186 insufficient amounts (below the threshold of detection), to its localization in other fractions of
187 the gradient that were not tested or to the fact that KCl treatment might have triggered its
188 dephosphorylation.
189

190 **Fig 2. Importance of IglB amino acid Y139 in sheath formation**

191 (**A**) Sucrose gradient. Lysates of bacteria grown in Schaedler K3 medium in the presence of
192 KCl were laid on top of a discontinuous sucrose gradient 15%-55%/Optiprep 55%. Left panel,
193 composition of the gradient; Right panel, transmission electron microscopy (TEM) of the
194 "heavy" fraction (grey arrow, topping the Optiprep cushion). The assembled sheath-like
195 structure, sedimenting at equilibrium to below 55% sucrose, showed rod-shaped particles of
196 variable length (100 - 600 nm). (**B**) Western blotting analysis of the different fractions, using
197 anti-Igl (A, B or C) antibodies. (**C**) Mass spectrometry analysis of the H and L fractions. Ratio
198 of the intensities of the proteins IglA, B and C detected in the H and the L fractions (H / L %).
199 (**D**) Proteome and phosphoproteome of cellular fractions. Intensities (in log2) of the non
200 phosphorylated (left) and phosphorylated (right) Tyr139-containing peptide in the "heavy" (H)
201 and "light" (L) fractions. The signal of the phosphopeptide was only detectable after
202 phosphoenrichment. nd, not detectable.

203

204 We decided to focus here on IglB and evaluate the importance of the phosphorylation on
205 Tyr139 on T6SS functionality and *Francisella* pathogenicity.

206

207 Comparative sequence analyses on 33 IglB proteins from 19 genomes of the *Francisella*
208 genus were performed to evaluate the conservation of residue Tyr139 (**S2 Fig**). All, but 5
209 genomes, encode two IglB proteins (due to the duplication of the FPI in these genomes).
210 Sequences were highly conserved between 31 IglB proteins sharing 93 to 100% amino acid
211 identity. In contrast, the proteins encoded by *FTN_0043,* encoded in another genomic island
212 termed the *F. novicida* island or FNI(42)) and *F7308_1917* (Fsp_TX077308) exhibit only 48%
213 amino acid identity with the 31 other IglB proteins whereas they both share 85% identity.
214 Excluding these 2 outliers, among 506 sites, 458 were without polymorphism (91%), with
215 Tyr139 conserved in all IglB sequences (**S2 Fig**). Of note, since IglB is among the most
216 conserved components of T6SS(30, 41) (**S1 Fig**) we were able to retrieve orthologues of IglB
217 encoded outside of *Francisella* genus. Out of 535 non-redundant IglB orthologues (also
218 named VipB, TssC or EvpB/VC_A0108), we found 90 sequences with a tyrosine in the
219 vicinity of Tyr139 site outside of *Francisella* genus. In 82 sequences, the predicted location of
220 the tyrosine residue was similar to that of Tyr139 (in a turn region between two helices) (**S2**
221 **Fig**).

222

223 **3D analysis**

224 Inspection of the 3.7 Å EM reconstruction of the *F. novicida* sheath[32] (PDB 3j9o) does not
225 show any atoms close enough to form a hydrogen bond with the hydroxyl of
226 Tyr139. However, the carboxylates of Asp114 from IglB, and Asp63 of IglA in the next dimer,
227 are around 5 Å away. At the resolution of the reconstruction, side chain positions are not
228 clearly defined and so these may approach close enough to Tyr139 OH to form hydrogen
229 bond interactions stabilizing the assembly.

230 There is space for a phosphate group on this atom as the OH is pointing into a pocket in
231 the structure (**Fig 3**). This was modeled by adding a phosphate group (using ccp4mg to
232 position a phosphate and then editing the PDB file to generate a PTR residue) onto the
233 hydroxyl and showing there were no steric clashes. However, the negatively charged

234 phosphate would induce charge repulsion with the nearby Asps from the next dimer most
235 likely preventing assembly of the strands when Tyr139 is phosphorylated.
236 Hence, the charge repulsion provoked by addition of the phosphogroup (when Y139 is
237 phosphorylated) is likely to weaken the stability of the assembled sheath.
238

239 **Fig 3. Predicted role of Y139 of IglB in sheath assembly**

240 (**A**) Overview of the sheath that consists of 12 helical strands based on EM reconstruction at
241 3.7 Å. Each unit consists of a IglA/IglB dimer. The same colors were used in the further
242 pictures. The chains near Tyr139 of IglB consist of 2 IglA/IglB dimers from the same strand
243 (pink/grey and coral/sky blue). The N-terminal tail of an IglA (blue) from an adjacent strand
244 wraps round to close to Y139 of this strand. (**B**) A closer view of just the selected chains.
245 (**C**) Close up of the region of Tyr139. The hydroxyl is pointing into a pocket and not
246 obviously making a Hydrogen bond. However, the carboxylates of Asp114 from IglB and
247 Asp63 of IglA in the next dimer are around 5 Å away. At the resolution of the reconstruction
248 side chain density is not well defined and these could in fact be close enough to H bond.
249 (**D**) Surface of the assembly clipped to show Tyr139. There is enough space for a Phospho
250 group on the Tyr. The two Asps will however be close to the phosphogroup and so there is
251 likely to be charge repulsion impairing the sheath assembly or weakening the sheath stability
252 when Y139 is phosphorylated.
253

254 **Role of IglB phosphorylation on IglA/IglB interaction and sheath formation**

255 We evaluated the importance of the phosphorylation site in IglB on T6SS assembly and
256 bacterial virulence by constructing two IglB variants in which Tyr139 was substituted either
257 by an alanine (Ala) or by the non-phosphorylatable aromatic analogue phenylalanine (Phe).
258 These IglB mutated proteins (designated Y139A and Y139F, respectively) were expressed *in*
259 *trans* in a Δ*iglB* mutant of *F. novicida* carrying a chromosomal deletion of the entire *iglB*

260 gene, (see Methods). A *F. novicida* mutant with a deletion of the entire *FPI*, unable to escape
261 from phagosomes and hence to grow in macrophages (43), was used as a negative control.
262 The mutations Y139A and Y139F had no effect on bacterial growth in broth (**S3 Fig**). The
263 impact of Y139A and Y139F substitutions was first tested by Western blotting on whole cell
264 lysates. As expected (**Fig 4A**), IglB was detected in wild-type and complemented strains but
265 not in the Δ*iglB* and Δ*FPI* strains. IglA was detected in all the strains, except the ΔFPI mutant,
266 but in clearly lower amounts in the Δ*iglB* strain. This observation is in agreement with earlier
267 observations (44), suggesting that the presence of IglB increases the stability of the IglA
268 protein.
269 A classical measure of basal T6SS function is the export of an Hcp-related protein.
270 Therefore, we examined IglB-dependent IglC export in the different *F. novicida* mutant
271 strains by Western-blot on bacteria grown in the presence -or absence- of 5% KCl. In
272 agreement with previous reports, IglC was detected in the culture supernatant in the
273 presence, but not in the absence, of KCl, in the wild-type and $iglB_{WT}$ complemented strains.
274 In contrast, deletion of *iglB* as well as the two single amino acid substitutions in IglB
275 abolished the secretion of IglC into the culture medium (**Fig 4B**), revealing that a wild-type
276 form of IglB is required for IglC secretion. KCl treatment did not modify the amounts of IglA,
277 IglB and IglC proteins detected by western blotting on whole cells (bacterial pellet fractions).
278 To test if any of the two substitutions at Tyr139 would impair IglA/IglB heterodimer
279 formation, we performed co-immunoprecipitation assays (**Fig 4C**), using either anti-IglA to
280 precipitate the complex, followed by western blotting with anti-IglB (upper panel) or anti-IglB,
281 followed by western blotting with anti-IglA (lower panel). In both assays, the two IglB mutant
282 alleles (Y139A and Y139F) were able to interact with IglA like wild-type IglB.
283 Since the presence of sheath-like structures correlated with the presence of non-
284 phosphorylated forms of IglB (**Fig 2**), we anticipated that the non-phosphorylatable Y139F
285 mutant might permanently produce oligomerized sheath-like structures. To test this
286 possibility, we performed sucrose gradient fractionation followed by western blotting (as
287 described previously) on the Y139F mutant strain. In contradiction of the above hypothesis,

288 the proteins IglA and IglB were detected in the L fractions of the gradient but not in the H
289 fraction corresponding to the sheath (**Fig 3D**) and no sheath-like structure could be
290 visualized by TEM in the H fraction of the Y139F mutant. Mass spectrometry analysis of the
291 fractions confirmed that only a very low portion of the IglA, B and C is present in the H
292 fractions compared to the L (**Fig 4E**). Since the only difference between the non-
293 phosphorylated form of Tyr139 and its non-phosphorylatable Phe analogue is the presence
294 of an additional hydroxyl moiety, it is likely that this hydroxyl contributes to sheath
295 formation/stability.
296

297 **Fig 4. Immunodetection**

298 (**A**) Western Blots (WB) of whole cell protein extracts. Upper gel: WB with anti-IglB; lower
299 gel: WB with anti-IglA. (**B**) Western Blots (WB) with anti-IglC on bacteria / culture filtrates.
300 Bacteria were grown in Schaedler-K3 supplemented or not with 5% KCl until late log phase
301 and then harvested by centrifugation. Culture supernatants were collected after filtration on
302 0.2 µM Millipore filters and concentrated using Amicon 3 kDa membranes. The equivalent of
303 200 µg of total protein were loaded onto each well. Upper gel, bacterial cultures grown
304 without KCl; lower gel, bacterial cultures supplemented with 5% KCl. (**C**) Co-
305 immunoprecipitations (Co-IP). Upper gel: IP-anti-IglA, followed by WB with anti-IglB; lower
306 gel: IP-anti-IglB, followed by WB with anti-IglA. (**D**) WBs of sucrose gradient fractions of the
307 Y139F mutant strain. Upper gel, WB with anti-IglB; Middle gel, WB with anti-IglA; lower gel,
308 WB with anti-IglC. (**E**) Mass spectrometry analysis of the H and L fractions of the Y139F
309 mutant strain. Ratio of the intensities of the proteins IglA, B and C detected in the H and the
310 L fractions (H / L %).
311

312 **Critical role of IglB residue Y139 in *Francisella* pathogenesis**

313 We next evaluated the impact of the Y139A and Y139F mutations on bacterial virulence by
314 studying their behavior in macrophages and in the mouse model. The ability of wild-type *F.*

315 *novicida* (WT), Δ*iglB* and complemented strains (CpWT, Y139A and Y139F) to survive and
316 multiply in murine macrophage-like J774.1 cells was monitored over a 24 h-period (**Fig 5A**).
317 Confirming earlier reports(45), intracellular multiplication of the Δ*iglB* mutant was essentially
318 abolished and comparable to that of the Δ*FPI* mutant. The single amino acid substitution of
319 Tyr139 by Ala (Y139A) was also sufficient to abolish intracellular bacterial multiplication. A
320 severe intracellular growth defect was also recorded when Tyr139 was substituted by Phe
321 (Y139F), until 10 h after infection (almost fifty-fold less bacterial counts). However, at 24 h,
322 the Y139F mutant strain multiplied and showed a ten-fold reduction of bacterial counts
323 compared to wild-type, suggesting that a late phagosomal escape had occurred in the Y139F
324 mutant, therefore promoting some cytosolic bacteria multiplication. As expected, functional
325 complementation (*i.e.,* introduction of a plasmid-born wild-type *iglB* allele into the Δ*iglB*
326 mutant strain (CpWT) restored wild-type growth.

327 We next tested the intracellular behavior of the Δ*iglB* mutant and complemented strains in
328 primary bone marrow-derived macrophages (BMMs). Growth of the Δ*iglB* deletion mutant as
329 well as that of the two Y139A or Y139F was identical to that of the Δ*FPI* mutant (**Fig 5B**) at
330 all time points tested. The fact that no multiplication of Y139F was recorded at 24 h is most
331 likely due to the higher bactericidal activity of primary macrophages compared to the J774-1
332 cell line. Functional complementation restored normal intracellular bacterial replication (in
333 CpWT).

334 The impact of the mutations in *iglB* on bacterial virulence was evaluated in an *in vivo*
335 competition assay between wild-type (WT) and Δ*iglB* mutant bacteria. For this, we monitored
336 the bacterial burden in spleen and livers 2.5 days after infection of 7-week-old female BALB/c
337 mice by the intra-peritoneal route (**Fig 5C**). The competition index recorded for the *iglB*
338 mutants (Y139A and Y139F) was very low ($\leq 10^{-6}$ in both target organs for Y139F; $\leq 10^{-5}$ in
339 livers and $\leq 10^{-6}$ in spleens for Y139A), demonstrating the importance of residue Tyr139 in
340 *Francisella* virulence in the mouse model. As a control, we also performed an *in vivo*
341 competition assay between wild-type and the Δ*iglB* complemented strain (WT and CpWT).
342 The competition index recorded close to 1 for CpWT ($\leq 10^{-1}$ in both target organs), confirmed

343 almost complete functional complementation.

344 To determine whether this lack of intracellular multiplication, associated with reduced
345 virulence, was due to impaired access to the host cytosol or aborted cytosolic multiplication,
346 we compared the ability of the Δ*iglB* mutants to escape from the phagosomal compartment to
347 that of the wild-type strain. For this, we first monitored co-localization of intracellular bacteria
348 with LAMP-1, in J774-1 macrophages (**Fig 5D**), using specific antibodies and automated
349 quantification (**Fig 5E**). The frequency of bacteria co-localizing with LAMP-1 at all 3 time
350 points was elevated (between 60% and 90%), with Δ*iglB* and the two complemented strains
351 expressing mutated *iglB* alleles (designated Y139A and Y139F; respectively). In contrast, co-
352 localization of the wild-type strain with LAMP-1 was below 20% after 1 h and remained in the
353 same range throughout the infection. These results strongly suggest that the Δ*iglB* mutant as
354 well as the two complemented strains expressing mutated *iglB* alleles, are still trapped in the
355 phagosomal compartment after 10 h, whereas the wild-type strain has already escaped into
356 the cytosol after 1 h.

357 The ability of the Δ*iglB* mutants to induce phagosomal membrane rupture was further
358 tested by using a CCF4 assay in BMMs, essentially as previously described(42, 46). Briefly,
359 bacteria were added to the macrophages at multiplicity of infection (MOI) of 100. After 1 h of
360 infection, cells were loaded for 1 h with CCF4. *F. novicida* naturally secretes β-lactamase
361 that is able to cleave the cytosolic CCF4 substrate. Once CCF4 is lysed, its emission
362 spectrum changes from 535 nm (green) to 450 nm (blue). Wild-type *F. novicida* and CpWT
363 strains showed similar amount of cleaved CCF4 at the three time-points tested (1 h, 3 h and
364 6 h) whereas there was no (or marginal) loss of FRET signal with Δ*iglB* (**Fig 5F**), Y139A,
365 Y139F, and in the two negative control strains Δ*FPI* and Δ*bla,* carrying a deletion of the
366 functional copy of the β-lactamase-encoding gene. These data confirmed that the two *iglB*
367 mutant strains (Y139A, Y139F) remained confined into intact phagosomes at least up to 6 h
368 after infection.

369

370 **Fig 5. IglB mutants show impaired intracellular survival and attenuated**
371 **virulence**

372 (**A, B**) Intracellular bacterial multiplication of wild-type *F. novicida* (WT, Grey squares),
373 isogenic Δ*iglB* mutant (Δ*iglB*, blue triangles) and complemented Δ*iglB* strain (Cp-WT, grey
374 circles; Y139A, blue square; Y139F, red squares) and the Δ*FPI* control (black lines), was
375 monitored during 24 h in J774A.1 macrophage cells (**A**) and bone marrow-derived
376 macrophages (BMDM) from BALB/c mice (**B**). In J774.1, the values recorded for Y139F, at
377 24 h, were significantly different from those of Δ*FPI*, Δ*iglB* or Y139A. In both cell types, the
378 values recorded for WT or CpWT, at 10 h and 24 h, were significantly different from those of
379 Δ*FPI*, Δ*iglB,* Y139A or Y139F. **p<0.001 (determined by student's t-test). (**C**) Groups of five
380 BALB/c mice were infected intraperitoneally with 100 CFU of wild-type *F. novicida* and 100
381 CFU of Δ*iglB* mutant strain or complemented strain (Cp-WT, Y139A, Y139F). Bacterial
382 burden was quantified in liver (L) and spleen (S) of mice. The data represent the competitive
383 index (CI) value (in ordinate) for CFU of mutant/wild-type of each mouse, after 48 h infection,
384 divided by CFU of mutant/wild-type in the inoculum. Bars represent the geometric mean CI
385 value. (**D, E**) Confocal microscopy of intracellular bacteria with J774-1 infected with wild-type
386 *F. novicida* (WT), Δ*iglB* or complemented strains and their co-localization with the
387 phagosomal marker LAMP1 observed at 1 h, 4 h and 10 h. J774.1 were stained for *F.*
388 *novicida* (green), LAMP-1 (red) and host DNA (blue, DAPI stained) (**D**). Analysis was
389 performed with ImageJ software (**E**). (**F**) CCF4 assay. Infection of *ASC*$^{-/-}$BMDM were
390 performed at MOI of 100 and the cytosol of BMDMs was loaded with CCF4, as described
391 previously(46). *F. novicida* naturally expresses a β-lactamase able to cleave the CCF4.
392 Bacterial escape into the host cytosol is thus associated with a shift of the CCF4 probe
393 fluorescence emission from 535 nm to 450 nm. The number of cells demonstrating CCF4
394 cleavage, determined at different time points (1 h, 3 h and 6 h) by flow cytometry, reached
395 above 50% at 6 h for both WT and CpWT complemented strains whereas it was below 1%
396 for the other mutant strains tested. *p<0.01 (determined by student's t-test).

397

398 Cytosolic escape of wild-type *F. novicida* is associated with the release of DNA that is
399 sensed by the host macrophage and triggers innate immune responses, namely secretion of
400 type I interferon (IFN), and activation of the AIM2 inflammasome (47-49). In contrast,
401 mutants that remain trapped in the phagosomal compartment generally fail to induce type I
402 IFN secretion (42). To check whether in spite of their phagosomal confinement, the *iglB*
403 mutants could still promote some cytosolic immune response, we quantified Type I IFN
404 secretion triggered upon infection with the *iglB* mutant strains, in supernatants of BMMs
405 infected for different time points (1 h, 3 h and 6 h; **Fig 6A**) by an ISRE-luciferase bioassay
406 (50). IFN secretion reached between 25 and 30 U/mL after 6 h, for both WT and CpWT
407 complemented strains whereas it remained below 5 U/mL for the other mutant strains tested,
408 further demonstrating that the *iglB* mutants remained trapped in phagosomes during the time
409 course of these assays.

410 Finally, cell death kinetics were determined to monitor possible cytotoxicity in infected
411 BMMs (measured by real time propidium iodide incorporation). Indeed, host cell death could
412 be an alternate explanation for the lack of bacterial intracellular multiplication. As expected,
413 delayed cell death (starting five hours after infection) was observed in BMM infected with
414 wild-type *F. novicida* (**Fig 6B**) as a result of normal intracellular bacterial multiplication and
415 activation of the AIM2 inflammasome. The Δ*iglB* complemented strain (CpWT) showed
416 similar cell death kinetics to the WT strain. In contrast, none of the other strains tested had
417 any substantial effect on BMM death, demonstrating that the intracellular multiplication
418 defects of the Y139A, Y139F mutant strains were not due to increased cytotoxicity and
419 further demonstrating that these mutants are likely to be stuck in intact phagosomes.

420

421 **Fig 6. Type I IFN secretion and cell death assays**

422 (**A**) Type I IFN secretion in the culture supernatant of BMDMs infected with the indicated
423 strains at an MOI of 1 was determined by the ISRE-luciferase bioassay and normalized using
424 rIFNβ. The supernatants of infections (50 μL) collected at different time points (1 h, 3 h and 6

425 h) were analyzed. Type I IFN secretion reached between 25 and 30 U/mL after 6 h, for both
426 WT and CpWT complemented strains whereas it remained below 5 U/mL for the other
427 mutant strains tested. (**B**) Cell death of BMDMs infected with the indicated strains at an MOI
428 of 1 was monitored in real time by monitoring propidium iodide fluorescence (expressed in
429 arbitrary units -AU) every 15 min. Mean and SD of triplicates from one experiment
430 representative of two independent experiments are shown in panels A, B. Unpaired t-tests
431 were performed, two-tailed P-values were $P \leq 0.001$.
432
433 These data demonstrated that residue Y139 of IglB is critical for functional T6SS
434 assembly, phagosomal escape and bacterial virulence and suggested that only the
435 unphosphorylated form of the protein was incorporated into sheath structures.
436 To verify that a residue possibly mimicking the phosphorylated state of Tyr139 would be
437 deleterious for functional T6SS assembly, we replaced Tyr139 by two phosphomimetics *i.e.*
438 the negatively charged amino acids Aspartate and Glutamate. We first evaluated the impact
439 of these amino acid substitutions (Y139D and Y139E) on intracellular multiplication in J774-1
440 cells (**S4 Fig**). The two mutants led to severe defects in intracellular multiplication and, at all
441 time points tested, the replication defect was comparable to that of the Y139A or Δ*FPI*
442 mutant. We next evaluated the capacity of the Y139D and Y139E mutants to form sheath-like
443 structure by using the sucrose gradient assay. In the two mutants, the IglB protein was
444 exclusively detected by Western blot in the L fractions of the sucrose gradient (**S4 Fig**),
445 strongly suggesting that the two amino acid substitutions at Tyr139 also prevented sheath-
446 like assembly.
447
448 Altogether, the data presented support the notion that dephosphorylated Tyr139 is
449 required for functional sheath assembly. Furthermore, they suggest that the free hydroxyl
450 group, present on the aromatic ring of the dephosphorylated form of Tyr139 (absent in the
451 Y139F mutant; **S4 Table**), plays an important role in the assembly of IglA/IglB oligomers.
452

453

454 # Discussion

455

456 We show here that phosphorylation status of IglB critically influences T6SS functional
457 assembly, bacterial phagosomal escape and virulence. This post-translational modification of
458 the sheath could constitute a mechanism controlling the dynamics of T6SS assembly.

459

460 **Phosphorylation of the sheath, a novel player in control of the T6SS**

461 Cryo-electron microscopy analyses (30) have demonstrated that the FPI of *F. novicida*
462 encodes a genuine T6SS and proposed a model in which the sheath of the T6SS is
463 composed of discs of heterodimers of inter-digitated IglA/IglB proteins. The dynamics of
464 T6SS sheaths have also been studied by live imaging approaches (8, 51 and references
465 therein). However, the molecular mechanisms associated with T6SS sheath contraction
466 remain speculative. Interestingly, the recently published structure of the sheath of one of
467 T6SS of *P. aeruginosa* (TssB1C1 from H1-T6SS) (52) suggests that the sheath shifts from
468 an extended state to a contracted state using a spring-like motion that might be conserved in
469 other T6SS.

470 Formation of the *Francisella* T6SS is believed to occur in the phagosome before cytosolic
471 escape of the bacterium. Nevertheless, T6SS elements are also likely to be required during
472 the cytosolic stage of the infectious cycle. Indeed, most FPI genes are induced during late
473 intra-macrophage growth (53) and IglC has been shown to be required for intracellular
474 growth of *F. novicida* that are microinjected directly into the cytosol of HeLa cells (54). IglC-
475 export in *F. novicida* depends on the T6SS core components IglA and IglB (55). Of note,
476 Clemens *et al*. (30) reported that some split-GFP fusions with truncated IglA proteins,
477 although still able to form IglA/IglB-heterodimers, had lost their IglC secretory function, which
478 suggests that heterodimer formation is not sufficient to generate a functional sheath.

479 Mass spectrometry analyses revealed that IglB contained a phosphorylated residue
480 (Tyr139). Remarkably, this residue was found in a phosphorylated form exclusively in non-

481 oligomerized IglB proteins, suggesting that the phosphorylation status of IglB residue Tyr139
482 could be instrumental in the biogenesis of a functional T6SS. The substitution of Tyr139
483 either by an alanine or by the non-phosphorylatable aromatic analogue phenylalanine still
484 allowed the interaction of IglA and IglB in co-immunoprecipitation assays. However, both
485 substitutions prevented secretion of IglC in the culture supernatant, revealing impaired T6SS
486 expression in these mutants. Fully supporting the notion that phosphorylation of Tyr139
487 impairs sheath assembly, replacement of this residue by a phosphomimetic (Y139D or
488 Y139E) led to a severe intracellular multiplication defect and prevented sheath-like structure
489 formation.

490 Our 3D predictions suggest that the OH of tyrosine, that is absent in the aromatic ring of
491 phenylalanine (**Fig 3 and S4 Table**), might be important for sheath formation. Upon addition
492 of a phosphoryl moiety at this position, charge repulsion between the phosphate group and
493 nearby aspartate residues would lead to the interaction between IglA and IglB being
494 destabilized. Therefore, phosphorylation is unfavorable for the formation of stable hexameric
495 rings and sheath-like structures. The fact that a late phagosomal escape of the Y139F
496 mutant apparently occurred in J774-1 macrophages (translated by some bacterial
497 multiplication at 24 h) tends to suggest that a partially active T6SS could still assemble in the
498 Y139F mutant.

499

500 **Possible regulatory mechanisms involved in tyrosine phosphorylation**

501 Protein phosphorylation on tyrosine is catalyzed by autophosphorylation of ATP-dependent
502 protein-tyrosine kinases (56). Bacterial tyrosine kinases do not share sequence homology
503 with eukaryotic tyrosine kinases (also called Hanks-type kinases) and, hence, have been
504 named BY-kinases. To date, the best-characterized function of BY-kinases is related to
505 capsular polysaccharide synthesis (57). Two main classes of bacterial tyrosine phosphatases
506 catalyze the reverse reaction: conventional eukaryotic-like phosphatases and low molecular
507 weight acidic phosphatases. *M. tuberculosis* possesses only one tyrosine kinase (PtkA), but
508 encodes two tyrosine phosphatases (PtpA and PtpB); the latter being also active against

509 phospho-Ser and phospho-Thr residues). These two tyrosine phosphatases have been
510 shown to act on host tyrosine signaling pathways. *S. aureus* also encodes one PtpA
511 orthologue (designated PtpA, sharing 32% amino acid identity with PtpA of *M. tuberculosis*)
512 that is phosphorylated by the tyrosine kinase CapA1B2 and secreted by the bacterium (57),
513 suggesting that, like in *M. tuberculosis*, the *S. aureus* PtpA protein could act as a host cell
514 signaling molecule(58).

515 As mentioned earlier, the *Francisella* genomes do not encode a canonical tyrosine kinase.
516 However, we identified a unique gene encoding a highly conserved protein (97.5% amino
517 acid identity between the different *F. tularensis* subsps), that is predicted be a low molecular
518 weight phosphotyrosine protein phosphatase (FTN_1046 in *F. novicida*). This protein,
519 designated PtpA, is composed of 161 amino acids and shares 40.1% amino acid identity with
520 its orthologue in *Staphylococcus aureus* (SAAG_02400), 29.2% with PtpA of *M.*
521 *tuberculosis* (TMBG_01746) and less than 28% amino acid identity with the tyrosine
522 phosphatase of *Escherichia coli* (Wzb and Etp(59); **S5 Fig**).

523 This prompted us to evaluate the impact of *ptpA* inactivation on *F. novicida* virulence,
524 using a *ptpA* transposon insertion mutant (from the *F. novicida* Tn insertion library (60). We
525 evaluated the capacity of the *ptpA* mutant to survive and multiply in J774.1 cells, over a 24 h-
526 period. We assumed that if PtpA served to dephosphorylate IglB, its inactivation would lead
527 to a constitutive production of sheath-like structures in this mutant that might affect normal
528 intracellular bacterial multiplication. The *ptpA* mutant multiplied in these cells like the wild-
529 type strain (**S5 Fig**). We also evaluated the functionality of the T6SS in this mutant by
530 monitoring IglC secretion in the supernatant of KCl-induced bacterial cultures and on the
531 formation of sheath-like structures by sucrose fractionation and western blotting. Confirming
532 the kinetics of intracellular multiplication, iglC secretion and T6SS assembly were similar in
533 the *ptpA* mutant to that of the wild-type strain. Altogether, these data strongly indicate that, in
534 *Francisella*, the protein PtpA does not play a role in T6SS assembly. At this stage, it cannot
535 be excluded that this putative phosphatase could play a similar function to its secreted
536 orthologues in *S. aureus* or *M. tuberculosis* that act on host proteins.

537 Thanks to the recent improvements in phosphoproteomic approaches, novel families of
538 protein kinases with a Ser/Thr/Tyr kinase activity have been identified (23). It is likely that
539 *Francisella* expresses non-canonical Ser/Thr/Tyr kinase-like activities that still await
540 authentication and characterisation.
541

542 **Structural and functional implications of IglB phosphorylation**

543 Tyrosine phosphorylation can regulate protein activity in multiple ways, including causing
544 electrostatic effects and allosteric transitions, but the most important function of
545 phosphotyrosine is to serve as a docking site for specific interaction with a target protein that
546 contains a phosphotyrosine binding domain. The Src homology 2 (SH2) domains represent
547 the largest class of known phosphotyrosine recognition domains in eukaryotic proteins (61)
548 and tyrosine phosphorylation serves to recruit SH2-containing targets.
549 Remarkably, no specific phosphotyrosine binding proteins have been found in bacteria.
550 Since the phosphate on Tyr is linked to the O^4 position of the phenolic ring, and therefore lies
551 much further away from the peptide backbone than the phosphate on the β-OH groups of
552 Ser and Thr, the effects of Tyr phosphorylation in bacteria may be exerted primarily through
553 allosteric/electrostatic effects. Looking at the full helical reconstruction, one can see that
554 Y139 is close to both D63 of IglA and D114 of IglB. These are from two different symmetry-
555 related chains (**Fig 3**). Putting a phosphate on Y139 is likely to repel the aspartate residues
556 and to disassemble the structure. Although, Aspartates and a Glutamate are not a likely
557 environment for a Phosphate, there is a quite large pocket which may be able to
558 accommodate the phosphate.
559 Since both Y139A and Y139F substitutions in IglB impaired secretion of IglC in the
560 supernatant of KCl-stimulated bacterial cultures (**Fig 6B**) and prevented normal phagosomal
561 escape in BMDM macrophages (**Figs 4 and 5**), it is clear that Tyr139 of IglB plays a critical
562 role in the functional assembly of the T6SS. Moreover, the fact that Y139F substitution also
563 prevented the formation of a sheath-like structure in KCl-stimulated bacteria, further indicates
564 that the presence of the non-phosphorylated OH moiety on the C4 of the phenol ring is also

565 important for proper assembly of the T6SS. The absence of phosphorylated IglB peptide
566 (carrying Y139p) in sheath like structures (**Fig 2C** and **S2 Table**), suggests that
567 phosphorylation of IglB is not favorable for sheath assembly (**Fig 7)**. Hence, it is tempting to
568 propose that modulating the phosphorylation status of IglB could represent a simple and
569 rapid mean for *Francisella* to regulate T6SS assembly/disassembly process (**Fig 7)**.
570

571 **Fig 7. Proposed model of phosphorylation-dependent TSS6 assembly-**
572 **disassembly**

573 (**Left**) Upon bacterial entry into the phagosomal compartment, phosphorylation of IglB may
574 decrease and non-phosphorylated IglB can form stable heterodimers with IglA. Sheath
575 assembly initiates at the bacterial pole. (**Right**) Within 30 min, T6SS sheath contraction
576 triggers the secretion of effectors and the rupture of the phagosomal membrane. Once in the
577 cytosol, the T6SS sheath disassembles, thanks to the concerted action of the ClpB unfoldase
578 and of the phosphorylation of IglB residue Y139.

579

580 Upon entry into the host cell phagosome, induced expression of IglB generated by
581 induction of the FPI (dephosphorylated form due to a reduced phosphorylation and/or
582 increased dephosphorylation) would promote T6SS assembly. Once in the cytosol,
583 phosphorylation of IglB (due to a reduced dephosphorylation and/or and increased
584 dephosphorylation) would then favor disassembly the contracted T6SS in concert with the
585 general stress chaperone ClpB (39) and allow active cytosolic bacterial multiplication. In the
586 Tyr139 mutant, bacteria remain trapped in the phagosome because of their inability to
587 promote efficient sheath assembly.

588 The post-translational phosphorylation of protein is a rapid and reversible mechanism.
589 Hence, yet unidentified phosphorylation-dependent mechanisms controlling the dynamics of
590 T6SS assembly might exist in other pathogens and should be carefully re-examined.
591

592

593 # Methods

594

595 **Ethics Statement**. All experimental procedures involving animals were conducted in
596 accordance with guidelines established by the French and European regulations for the care
597 and use of laboratory animals (Decree 87–848, 2001–464, 2001–486 and 2001–131 and
598 European Directive 2010/63/UE) and approved by the INSERM Ethics Committee
599 (Authorization Number: 75-906).

600

601 **Strains and culture conditions**

602 All strains used in this study are derived from *F. tularensis* subsp. *novicida* U112 (*F. novicida*)
603 as described in **Supplementary Table 5**. Strains were grown at 37°C on pre-made chocolate
604 agar PolyViteX plates (BioMerieux), Schaedler K3 or Chemically Defined Medium (CDM).
605 The CDM used for *F. novicida* corresponds to standard CDM (62) without threonine and
606 valine (63). For growth condition determination, bacterial strains were inoculated in the
607 appropriate medium at an initial OD_{600} of 0.05 from an overnight culture in Schaedler K3
608 medium.

609

610 **Construction of a Δ*iglB* deletion mutant**

611 We inactivated the gene *iglB* in *F. novicida* (*FTN_1323*) by allelic replacement resulting in the
612 deletion of the entire gene (4 first codons and 7 last codons were conserved). We
613 constructed a recombinant PCR product containing the upstream region of the gene *iglB*
614 (*iglB*-UP), a kanamycin resistance cassette (*nptII* gene fused with *pGro* promoter) and the
615 downstream region of the gene *iglB* (*iglB*-DN) by overlap PCR. Primers *iglB* upstream FW
616 (p1) and *iglB* upstream (spl_K7) RV (p2) amplified the 689 bp region upstream of position +3
617 of the *iglB* coding sequence (*iglB*-UP), primers *pGro* FW (p3) and *nptII* RV (p4) amplified the
618 1091 bp kanamycin resistance cassette (*nptII* gene fused with *pGro* promoter); and primers

619 *iglB* downstream (spl_K7) FW (p5) and *iglB* downstream RV (p6) amplified the 622 bp region
620 downstream of the position +1520 of the *iglB* gene coding sequence (*iglB*-DN). Primers p2
621 and p5 have an overlapping sequence of 12 nucleotides with primers p3 and p4 respectively
622 resulting in fusion of *iglB*-UP and *iglB*-DN with the cassette after cross-over PCR. All single
623 fragment PCR reactions were realized using Phusion High-Fidelity DNA Polymerase
624 (ThermoScientific) and PCR products were purified using NucleoSpin® Gel and PCR Clean-
625 up kit (Macherey-Nagel). Overlap PCRs were carried out using 100 ng of each purified PCR
626 products and the resulting fragment of interest was purified from agarose gel. This fragment
627 was then directly used to transform wild type *F. novicida* by chemical transformation (64).
628 Recombinant bacteria were isolated on Chocolate agar plates containing kanamycin (10 µg
629 mL^{-1}). The mutant strains were checked for loss of the wild type gene by PCR product direct
630 sequencing (GATC-biotech) using appropriate primers.
631

632 **Functional complementation**

633 The Δ*iglB* mutant strain was transformed with the recombinant pKK214-derived plasmids
634 (pKK-*iglBY139A*$_{cp}$, pKK-*iglBY139F*$_{cp}$, pKK-*iglBY139D*$_{cp}$ and pKK-*iglBY139E*$_{cp}$) described
635 below (**Supplementary Table 5**). Primers pGro(65) FW and pGro RV amplified the 328 bp of
636 the *pGro* promoter and primers *iglB* FW / *iglB*[PstI] RV amplified the 1,534 bp *iglB* gene from
637 U112. PCR products were purified and SmaI (*pGro* promoter) or PstI (*iglB*) digested in
638 presence of FastAP Thermosensitive Alkaline Phosphatase (ThermoScientific) to avoid self-
639 ligation. Mixtures of *pGro* promoter and fragments of the genes of interest were then
640 incubated with T4 DNA Ligase (New England Biolabs) to allow blunt end ligation and
641 fragments were then cloned in pKK214 vector after SmaI/PstI double digest and transformed
642 in *E. coli* TOP10. Recombinant plasmid pKK-*iglB*$_{cp}$ was purified and directly used for
643 chemical transformation in *F. novicida* Δ*iglB* (64). Recombinant colonies were selected on
644 Chocolate agar plates containing tetracycline (5 µg mL^{-1}) and kanamycin (10 µg mL^{-1}).
645

646 For site-directed mutagenesis of *iglB* gene, we used plasmid pKK-*iglB*$_{cp.}$ The recombinant
647 plasmids pKK-*iglBY139A*$_{cp}$, pKK-*iglBY139F*$_{cp}$, pKK-*iglBY139D*$_{cp}$ and pKK-*iglBY139E*$_{cp}$ were
648 constructed using the primer pairs iglB (Y/A, Y/F,Y/D, or Y/E) FW and iglB RV
649 (**Supplementary Table 6**). The three first bases of primers iglB FW were modified to change
650 Tyr139 to Ala, Phe, Asp or Glu
651 PCR products were purified, phosphorylated by the T4 Polynucleotide Kinase and then
652 incubated with T4 DNA Ligase (New England Biolabs) and transformed in *E. coli* TOP10.
653 Recombinant plasmids were purified and directly used for chemical transformation in *F.*
654 *novicida* Δ*iglB*, as described previously (64). Recombinant colonies were selected on
655 Chocolate agar plates containing tetracycline (5 µg mL^{-1}) and kanamycin (10 µg mL^{-1}).
656

657 **Immunodetection**

658 Antibodies to IglA, IglB and IglC were obtained through the NIH Biodefense and Emerging
659 Infections (BEI) Research Resources Repository, NIAID, NIH.
660 **Immunoblotting analysis.** Protein lysates for immunoblotting were prepared by using
661 Laemmli sample buffer. Protein lysates corresponding to equal OD_{600} were loaded on 12%
662 Bis/Tris gels (Invitrogen), and run in TGS buffer. Primary antibodies (anti-IglA or anti-IglB)
663 were used at final dilution of 1:2,000. Secondary horseradish peroxidase (HRP)-conjugated
664 goat anti-mouse antibody (Santa Cruz Biotechnology, CA, USA) or (HRP)-conjugated goat
665 anti-rabbit antibody and the enhanced Chemiluminescence system (ECL) (Amersham
666 Biosciences, Uppsala, Sweden) were used as previously described (66).
667 **Co-immunoprecipitations**. Wild-type *F. novicida* was grown to late exponential phase in
668 Schaedler K3; collected by centrifugation and lysed with lysozyme and 1% TritonX-100
669 detergent in 20 mM Tris HCl, (pH 7.8) with 1 mM EDTA, protease inhibitor cocktail and
670 benzonase nuclease. The lysate was centrifuged at 15,000 g for 15 min at 4°C to pellet
671 bacterial debris. Monoclonal anti-IglB antibody was incubated 40 min with Dynabeads protein
672 G (Invitrogen) and the complex was incubated at room temperature with the bacterial lysate

673 for 1 hour. After washing, the complex was loaded on 12% Bis/Tris gels (Invitrogen), and run
674 in TGS buffer.
675
676 **Purification of T6SS**
677 T6SS were prepared essentially as described in (30). Briefly, wild-type *F. novicida* was
678 grown to late exponential phase in Schaedler K3 containing 5% KCl; pelleted by
679 centrifugation and lysed with lysozyme and 1% TritonX-100 detergent in 20 mM Tris HCl, (pH
680 7.8) with 1 mM EDTA, protease inhibitor cocktail and benzonase nuclease. The lysate was
681 centrifuged 3 times at 15,000 g for 30 min at 4°C to pellet bacterial debris, and the
682 supernatant was layered onto a 10%–55% sucrose gradient overlying a 55% Optiprep
683 cushion and centrifuged at 100,000 g for 18 hr. Fractions were collected and examined by
684 TEM negative staining using 2% uranyl acetate. The sheath-like structures sedimented to
685 just below the 55% sucrose/Optiprep interface.
686
687 **Phosphoproteomic analyses**
688 **Reagents and chemicals.** For protein digestion, dithiothreitol, iodoacetamide and
689 ammonium bicarbonate were purchased from Sigma-Aldrich (St Louis, MO, USA). For
690 phosphopeptide enrichment and LC-MS/MS analysis, trifluoroacetic acid (TFA), formic acid,
691 acetonitrile and HPLC-grade water were purchased from Fisher Scientific (Pittsburgh, PA,
692 USA) at the highest purity grade.
693 **Protein digestion.** For proteomic analysis, *F. novicida* was analysed in three independent
694 biological replicates. Protein concentration was determined by DC assay (Biorad, CA, USA)
695 according to the manufacturer's instructions. An estimated 1.2 mg of proteins for each
696 biological replicates were digested following a FASP protocol (67) slightly modified. Briefly,
697 proteins were reduced using 100 mM dithiothreitol in 50 mM ammonium bicarbonate for 1h at
698 60°C. Proteins were then split into four samples of 300 µg and applied on 30 kDa MWCO
699 centrifugal filter units (Microcon, Millipore, Germany, Cat No MRCF0R030). Samples were

700 mixed with 200 µL of 8M urea in 50 mM ammonium bicarbonate (UA buffer) and centrifuged
701 for 20 min at 15,000 x g. Filters were washed with 200 µL of UA buffer. Proteins were
702 alkylated for 30min by incubation in the dark at room temperature with 100 µL of 50 mM
703 iodoacetamide in UA buffer. Filters were then washed twice with 100 µL of UA buffer (15,000
704 x g for 15 min) followed by two washes with 100 µL of 50 mM ammonium bicarbonate
705 (15,000 x g for 10 min). Finally, sequencing grade modified trypsin (Promega, WI, USA) was
706 added to digest the proteins in 1:50 ratio for 16 h at 37°C. Peptides were collected by
707 centrifugation at 15,000 x g for 10min followed by one wash with 50mM ammonium
708 bicarbonate and vacuum dried.

709 **Phosphopeptides enrichment by titanium dioxide (TiO_2) and phosphopeptides**
710 **purification by graphite carbon (GC).** Phosphopeptide enrichment was carried out using a
711 Titansphere TiO_2 Spin tip (3 mg/200 µL, Titansphere PHOS-TiO, GL Sciences Inc, Japan) an
712 estimated 1.2 mg of digested proteins for each biological replicate. Briefly, the TiO_2 Spin tips
713 were conditioned with 20 µL of solution A (80% acetonitrile, 0,1% TFA), centrifuged at 3,000
714 x g for 2min and equilibrated with 20µL of solution B (75% acetonitrile, 0,075% TFA, 25%
715 lactic acid) followed by centrifugation at 3,000 x g for 2 min. Peptides were resuspended in
716 10 µL of 2% TFA, mixed with 100 µL of solution B and centrifuged at 1,000 x g for 10min.
717 Sample was applied back to the TiO_2 Spin tips two more times in order to increase the
718 adsorption of the phosphopeptides to the TiO_2. Spin tips were washed with, sequentially, 20
719 µL of solution B and two times with 20 µL of solution A. Phosphopeptides were eluted by the
720 sequential addition of 50 µL of 5% NH_4OH and 50 µL of 5% pyrrolidine. Centrifugation was
721 carried out at 1,000 x g for 5 min.

722 Phosphopeptides were further purified using GC Spin tips (GL-Tip, Titansphere, GL Sciences
723 Inc, Japan). Briefly, the GC Spin tips were conditioned with 20 µL of solution A, centrifuged
724 at 3,000 x g for 2 min and equilibrated with 20 µL of solution C (0,1% TFA in HPLC-grade
725 water) followed by centrifugation at 3,000 x g for 2 min. Eluted phosphopeptides from the
726 TiO_2 Spin tips were added to the GC Spin tips and centrifuged at 1,000 x g for 5 min. GC

727 Spin tips were washed with 20 µL of solution C. Phosphopeptides were eluted with 70 µL of
728 solution A (1,000 x g for 3 min) and vacuum dried.
729 **nanoLC-MS/MS protein identification and quantification.** Samples were resuspended in
730 12 µL of 0.1% TFA in HPLC-grade water. For each run, 5 µL was injected in a nanoRSLC-Q
731 Exactive PLUS (RSLC Ultimate 3000, Thermo Scientific, MA, USA). Phosphopeptides were
732 loaded onto a µ-precolumn (Acclaim PepMap 100 C18, cartridge, 300 µm i.d.×5 mm, 5 µm,
733 Thermo Scientific, MA, USA) and were separated on a 50 cm reversed-phase liquid
734 chromatographic column (0.075 mm ID, Acclaim PepMap 100, C18, 2 µm, Thermo Scientific,
735 MA, USA). Chromatography solvents were (A) 0.1% formic acid in water, and (B) 80%
736 acetonitrile, 0.08% formic acid. Phosphopeptides were eluted from the column with the
737 following gradient 5% to 40% B (180 min), 40% to 80% (6 min). At 181 min, the gradient
738 returned to 5% to re-equilibrate the column for 20 minutes before the next injection. Two
739 blanks were run between each sample to prevent sample carryover. Phosphopeptides
740 eluting from the column were analyzed by data dependent MS/MS, using top-8 acquisition
741 method. Phosphopeptides were fragmented using higher-energy collisional dissociation
742 (HCD). Briefly, the instrument settings were as follows: resolution was set to 70,000 for MS
743 scans and 17,500 for the data dependent MS/MS scans in order to increase speed. The MS
744 AGC target was set to 1 x 10^6 counts with maximum injection time set to 250 ms, while
745 MS/MS AGC target was set to 2 x 10^5 with maximum injection time set to 250 ms. The MS
746 scan range was from 400 to 1.800 m/z. MS and MS/MS scans were recorded in profile
747 mode. Dynamic exclusion was set to 30 seconds.
748
749 **Data Processing Following nanoLC-MS/MS acquisition.** The MS files were processed
750 with the MaxQuant software version 1.5.3.30 and searched with Andromeda search engine
751 against the UniProtKB/Swiss-Prot *F. tularensis* subsp. *novicida* database (release 28-04-
752 2014, 1719 entries). To search parent mass and fragment ions, we set an initial mass
753 deviation of 4.5 ppm and 0.5 Da respectively. The minimum peptide length was set to 7
754 amino acids and strict specificity for trypsin cleavage was required, allowing up to two missed

755 cleavage sites. Carbamidomethylation (Cys) was set as fixed modification, whereas oxidation
756 (Met), N-term acetylation and phosphorylation (Ser, Thr, Tyr) were set as variable
757 modifications. The match between runs option was enabled with a match time window of 0.7
758 min and an alignment time window of 20 min. The false discovery rates (FDRs) at the protein
759 and peptide level were set to 1%. Scores were calculated in MaxQuant as described
760 previously(68). The reverse and common contaminants hits were removed from MaxQuant
761 output.

762 The phosphopeptides output table and the corresponding logarithmic intensities were used
763 for phosphopeptide analysis. The phosphopeptide table was expanded to separate individual
764 phosphosites, and we kept all sites identified at least once in the three independent
765 replicates of the analysis of *F. novicida*.

766 All data analysis of mass spectrometry data was performed in Perseus 1.6.0.7. For functional
767 class annotation, we also integrated COG and EggNog databases in Perseus 1.6.0.7, freely
768 available at www.perseus-framework.org. Data are available via ProteomeXchange with
769 identifier PXD009225.

770

771 **Cell cultures and cell infection experiments**

772 J774A.1 (ATCC® TIB-67™) cells were propagated in Dulbecco's Modified Eagle's Medium
773 (DMEM, PAA), containing 10% fetal bovine serum (FBS, PAA) unless otherwise stated. The
774 day before infection, approximately $2x10^5$ eukaryotic cells per well were seeded in 12-well
775 cell tissue plates and bacterial strains were grown overnight in 5 mL of Schaedler K3 at
776 37°C. Infections were realized at a multiplicity of infection (MOI) of 100 and incubated for 1 h
777 at 37°C in culture medium. After 3 washes with cellular culture medium, plates were
778 incubated for 4, 10 and 24 h in fresh medium supplemented with gentamycin (10 µg mL^{-1}). At
779 each kinetic point, cells were washed 3 times with culture medium and lysed by addition of 1
780 mL of distilled water for 10 min at 4°C. The titre of viable bacteria was determined by

781 spreading preparations on chocolate plates. Each experiment was conducted at least twice
782 in triplicates.
783
784 **Confocal experiments**
785 J774.1 macrophage cells were infected (MOI of 1,000) with wild-type *F. novicida* U112, the
786 isogenic Δ*iglB* mutant, the Δ*iglB* complemented either with wild-type *iglB* (CpWT) Y139A,
787 Y139F mutants or an isogenic Δ*FPI* strain, in standard DMEM (DMEM-glucose) for 30 min at
788 37°C. Cells were then washed three times with PBS and maintained in fresh DMEM
789 supplemented with gentamycin (10 μg mL^{-1}) until the end of the experiment. Three kinetic
790 points (*i.e.* 1 h, 4 h and 10 h) were sampled. For each time point, cells were washed with 1X
791 PBS, fixed 15 min with 4% paraformaldheyde, and incubated 10 min in 50 mM NH_4Cl in 1X
792 PBS to quench free aldehydes. Cells were then blocked and permeabilised with PBS
793 containing 0.1% saponin and 5% goat serum for 10 min at room temperature. Cells were
794 then incubated for 30 min with anti-*F. novicida* mouse monoclonal antibody (1/500e final
795 dilution, Creative Diagnostics) and anti-LAMP1 rabbit polyclonal antibody (1/100e, ABCAM).
796 After washing, cells were incubated for 30 min with Alexa488-conjugated goat anti mouse
797 and Alexa546 conjugated donkey anti rabbit secondary antibodies (1/400e, AbCam). After
798 washing, DAPI was added (1/1,000) for 1 min and glass coverslips were mounted in Mowiol
799 (Cityfluor Ltd.). Cells were examined using an X63 oil-immersion objective on a Zeiss
800 Apotome 2 microscope. Co-localisation tests were quantified by using Image J software; and
801 mean numbers were calculated on more than 500 cells for each condition. Confocal
802 microscopy analyses were performed at the Cell Imaging Facility (Faculté de Médecine
803 Necker Enfants-Malades).
804
805 **BMDMs Infections**
806 Infection of WT or *ASC*$^{-/-}$ BMDMs was performed as described previously (42). Briefly,
807 BMDMs were differentiated in DMEM (Invitrogen) with 10% v/v FCS (Thermo Fisher

808 Scientific), 15% MCSF (L929 cell supernatant), 10 mM HEPES (Invitrogen), and non-
809 essential amino acids (Invitrogen). One day before infection, macrophages were seeded into
810 12- 48- or 96-well plates at a density of 2 x10^5, 1.5 x10^5 or 5 x10^4 cells per well, respectively
811 and incubated at 37°C, 5% CO_2. The overnight culture of bacteria was added to the
812 macrophages at multiplicity of infection (MOI) of 100. The plates were centrifuged for 15 min
813 at 500 g to ensure comparable adhesion of the bacteria to the cells and placed at 37°C for
814 1h. After 3 washes with PBS, fresh medium with 5 µg mL^{-1} gentamycin (Invitrogen) was
815 added to kill extracellular bacteria and plates were incubated for the desired time.
816

817 **Phagosomal rupture assay**

818 Quantification of vacuolar escape using the β-lactamase/CCF4 assay (Life technologies) was
819 performed as previously described(49). *ASC*$^{-/-}$ BMDMs seeded onto non-treated plates were
820 infected as described above for 2 h, washed and incubated in CCF4 for 1 h at room
821 temperature in the presence of 2.5 mM probenicid (Sigma). Propidium iodide negative cells
822 were considered for the quantification of cells containing cytosolic *F. novicida* using
823 excitation at 405 nm and detection at 450 nm (cleaved CCF4) or 510 nm (intact CCF4).
824

825 **Type I IFN secretion**

826 Type I IFN secretion was determined in *ASC*$^{-/-}$ BMDMs by an ISRE-luciferase bioassay(50).
827 L929 ISRE-luciferase cells were plated at 5x10^4 cells per well in a 96 wells-plate and
828 incubated 24 h at 37°C with 5% CO_2. 50 µl of supernatants from infected BMDMs were
829 added for 4 h onto the ISRE-luciferase cells. Luciferase luminescence was detected using
830 Bright Glo Assay (Promega) following the manufacturer's instructions. Mouse rINF-β was
831 used as standard to determine the concentration of type I IFN in each sample.
832

833 **Cell death assays**

834 After infection 1h at MOI=100, WT BMMs were washed 3 times and incubated with
835 Propidium Iodide (PI; 5 µg mL^{-1}) in CO_2-independent medium (ThermoFisher Scientific). PI
836 incorporation was determined by measuring the fluorescence emission at 635 nm every 15
837 min on a microplate fluorescent reader (Tecan).
838

839 **Mouse infection**

840 Wild-type *F. novicida*, the Δ*iglB* mutant and the Δ*iglB* mutant complemented either with wild-
841 type *iglB* (CpWT) or with Y139A and Y139F mutants, were grown in Schaedler K3 to
842 exponential growth phase and diluted to the appropriate concentrations. 6 to 8-week-old
843 female BALB/c mice (Janvier, Le Genest St Isle, France) were intraperitoneally (i.p.)
844 inoculated with 200 µL of bacterial suspension. The actual number of viable bacteria in the
845 inoculum was determined by plating dilutions of the bacterial suspension on chocolate plates.
846 For competitive infections, wild-type *F. novicida* and mutant bacteria were mixed in 1:1 ratio
847 and a total of 100 bacteria were used for infection of each of five mice. After two days, mice
848 were sacrificed. Homogenized spleen and liver tissue from the five mice in one experiment
849 were mixed, diluted and spread on to chocolate agar plates. Kanamycin selection to
850 distinguish wild-type and mutant bacteria was performed. Competitive index (CI) [(mutant
851 output/WT output)/(mutant input/WT input)]. Statistical analysis for CI experiments was as
852 described in (69). Macrophage experiments were analyzed by using the Student's unpaired t
853 test.
854

855 **Sequence analyses**

856 To retrieve IglB homologous proteins, we used the Hidden Markov Model (HMM) profile
857 "T6SSii_iglB.hmm" from reference (32). We scanned a dataset of 2,462 predicted proteomes
858 of complete bacterial genomes retrieved from GenBank Refseq (last accessed September
859 2016)(70) using *hmmsearch* program of HMMER v.3.1b2 (gathering threshold = 25).

860 Our dataset included 19 genomes of the *Francisella* genus. All IglB sequences encoded by
861 *Francisella* genomes were aligned with MUSCLE v.3.8.31(71). Due to differences in the
862 annotation of the first methionine codon, we used the sequence of FTN_1323 as a reference
863 for the multiple sequence alignment.

864 Redundancy of the sequence set retrieved from *hmmsearch* was reduced using cd-hit-
865 v4.6.7 (72) with a 90% identity threshold. The longest representative sequence of each
866 cluster was then aligned with MUSCLE v.3.8.31 (71). Outliers that were very divergent in
867 sequence length were removed. PROMALS3D and ESPript3.0 (73) servers were used to
868 visualize multiple sequence and structure alignment using 3J9O.B PDB structure reference
869 file(30). To determine the conservation of the phosphotyrosine site identified in *Francisella*
870 genus (Tyr139 or Y139) we focused on the 12 amino acids surrounding the *Francisella*
871 Tyr139 residue in the 535 aligned sequences.

872 To determine the conservation of the phosphotyrosine site identified in *Francisella* genus
873 (Tyr139) we focused on the 12 amino acids surrounding the *Francisella* Y139 residue in the
874 535 aligned sequences. Out of the 535 aligned sequences, we found 90 sequences with a
875 tyrosine residue in the vicinity of *Francisella* Tyr139 residue. For illustrative purpose, we
876 selected 12 representative sequences out of 90 as shown in **Fig. 2D**.

877

878 ## Data Availability

879 The mass spectrometry proteomics data have been deposited in the ProteomeXchange
880 Consortium via the PRIDE (74) partner repository with the dataset identifier PXD009225.

881

882

883

884

885

886 # Acknowledgements

887 We thank Dr A. Sjostedt for providing the *Francisella* strain U112 and its *ptpA* transposon
888 insertion derivative (*FTN_1046*) and Alain Schmitt (Cochin Institute Electron Microscopy
889 Facility) for excellent technical support.

890

891

References

892 1. Sjostedt A. Tularemia: history, epidemiology, pathogen physiology, and clinical
893 manifestations. Ann N Y Acad Sci. 2007;1105:1-29.
894 2. Sjostedt A, editor. Francisella tularensis and tularemia: Fontiers Media SA; 2011.
895 3. Luque-Larena JJ, Mougeot F, Arroyo B, Vidal MD, Rodriguez-Pastor R, Escudero R,
896 et al. Irruptive mammal host populations shape tularemia epidemiology. PLoS Pathog.
897 2017;13(11):e1006622.
898 4. Maurin M, Gyuranecz M. Tularaemia: clinical aspects in Europe. Lancet Infect Dis.
899 2016;16(1):113-24.
900 5. Santic M, Molmeret M, Klose KE, Abu Kwaik Y. Francisella tularensis travels a novel,
901 twisted road within macrophages. Trends Microbiol. 2006;14(1):37-44.
902 6. McLendon MK, Apicella MA, Allen LA. Francisella tularensis: taxonomy, genetics, and
903 Immunopathogenesis of a potential agent of biowarfare. Annu Rev Microbiol. 2006;60:167-
904 85.
905 7. Kingry LC, Petersen JM. Comparative review of Francisella tularensis and Francisella
906 novicida. Front Cell Infect Microbiol. 2014;4:35.
907 8. Brodmann M, Dreier RF, Broz P, Basler M. Francisella requires dynamic type VI
908 secretion system and ClpB to deliver effectors for phagosomal escape. Nat Commun.
909 2017;8:15853.

910 9. Eshraghi A, Kim J, Walls AC, Ledvina HE, Miller CN, Ramsey KM, et al. Secreted
911 Effectors Encoded within and outside of the Francisella Pathogenicity Island Promote
912 Intramacrophage Growth. Cell Host Microbe. 2016;20(5):573-83.
913 10. Lagrange B, Benaoudia S, Wallet P, Magnotti F, Provost A, Michal F, et al. Human
914 caspase-4 detects tetra-acylated LPS and cytosolic Francisella and functions differently from
915 murine caspase-11. Nat Commun. 2018;9(1):242.
916 11. Charity JC, Blalock LT, Costante-Hamm MM, Kasper DL, Dove SL. Small molecule
917 control of virulence gene expression in Francisella tularensis. PLoS Pathog.
918 2009;5(10):e1000641.
919 12. Charity JC, Costante-Hamm MM, Balon EL, Boyd DH, Rubin EJ, Dove SL. Twin RNA
920 polymerase-associated proteins control virulence gene expression in Francisella tularensis.
921 PLoS Pathog. 2007;3(6):e84.
922 13. Cuthbert BJ, Ross W, Rohlfing AE, Dove SL, Gourse RL, Brennan RG, et al.
923 Dissection of the molecular circuitry controlling virulence in Francisella tularensis. Genes
924 Dev. 2017;31(15):1549-60.
925 14. Meibom KL, Forslund AL, Kuoppa K, Alkhuder K, Dubail I, Dupuis M, et al. Hfq, a
926 novel pleiotropic regulator of virulence-associated genes in Francisella tularensis. Infect
927 Immun. 2009;77(5):1866-80.
928 15. Meibom KL, Barel M, Charbit A. Loops and networks in control of Francisella
929 tularensis virulence. Future Microbiol. 2009;4:713-29.
930 16. Celli J, Zahrt TC. Mechanisms of Francisella tularensis intracellular pathogenesis.
931 Cold Spring Harb Perspect Med. 2013;3(4):a010314.
932 17. Ziveri J, Barel M, Charbit A. Importance of Metabolic Adaptations in Francisella
933 Pathogenesis. Front Cell Infect Microbiol. 2017;7:96.
934 18. Balonova L, Mann BF, Cerveny L, Alley WR, Chovancova E, Forslund AL, et al.
935 Characterization of protein glycosylation in Francisella tularensis subsp. holarctica;
936 identification of a novel glycosylated lipoprotein required for virulence. Mol Cell Proteomics.
937 2012;11(7):M111.015016.

938 19. Dankova V, Balonova L, Link M, Straskova A, Sheshko V, Stulik J. Inactivation of
939 Francisella tularensis Gene Encoding Putative ABC Transporter Has a Pleiotropic Effect
940 upon Production of Various Glycoconjugates. J Proteome Res. 2016;15(2):510-24.
941 20. Barel M, Charbit A. Role of Glycosylation/Deglycolysation Processes in Francisella
942 tularensis Pathogenesis. Front Cell Infect Microbiol. 2017;7:71.
943 21. Canova MJ, Molle V. Bacterial serine/threonine protein kinases in host-pathogen
944 interactions. J Biol Chem. 2014;289(14):9473-9.
945 22. Shi L, Pigeonneau N, Ravikumar V, Dobrinic P, Macek B, Franjevic D, et al. Cross-
946 phosphorylation of bacterial serine/threonine and tyrosine protein kinases on key regulatory
947 residues. Front Microbiol. 2014;5:495.
948 23. Nguyen HA, El Khoury T, Guiral S, Laaberki MH, Candusso MP, Galisson F, et al.
949 Expanding the Kinome World: A New Protein Kinase Family Widely Conserved in Bacteria. J
950 Mol Biol. 2017;429(20):3056-74.
951 24. Deutscher J, Ake FM, Derkaoui M, Zebre AC, Cao TN, Bouraoui H, et al. The
952 bacterial phosphoenolpyruvate:carbohydrate phosphotransferase system: regulation by
953 protein phosphorylation and phosphorylation-dependent protein-protein interactions.
954 Microbiol Mol Biol Rev. 2014;78(2):231-56.
955 25. Rodionova IA, Zhang Z, Mehla J, Goodacre N, Babu M, Emili A, et al. The
956 phosphocarrier protein HPr of the bacterial phosphotransferase system globally regulates
957 energy metabolism by directly interacting with multiple enzymes in Escherichia coli. J Biol
958 Chem. 2017;292(34):14250-7.
959 26. Meibom KL, Charbit A. Francisella tularensis metabolism and its relation to virulence.
960 Front Microbiol. 2010;1:140.
961 27. Dai S, Mohapatra NP, Schlesinger LS, Gunn JS. Regulation of Francisella tularensis
962 virulence. Frontiers in Microbiology. 2011;2.
963 28. Alkhuder K, Meibom KL, Dubail I, Dupuis M, Charbit A. Identification of trkH,
964 Encoding a Potassium Uptake Protein Required for Francisella tularensis Systemic
965 Dissemination in Mice. PLoS One. 2010;5(1):e8966.

966 29. Bell BL, Mohapatra NP, Gunn JS. Regulation of virulence gene transcripts by the
967 Francisella novicida orphan response regulator PmrA: role of phosphorylation and evidence
968 of MglA/SspA interaction. Infect Immun. 2010;78(5):2189-98.
969 30. Clemens DL, Ge P, Lee BY, Horwitz MA, Zhou ZH. Atomic structure of T6SS reveals
970 interlaced array essential to function. Cell. 2015;160(5):940-51.
971 31. Russell AB, Wexler AG, Harding BN, Whitney JC, Bohn AJ, Goo YA, et al. A type VI
972 secretion-related pathway in Bacteroidetes mediates interbacterial antagonism. Cell Host
973 Microbe. 2014;16(2):227-36.
974 32. Abby SS, Cury J, Guglielmini J, Neron B, Touchon M, Rocha EP. Identification of
975 protein secretion systems in bacterial genomes. Sci Rep. 2016;6:23080.
976 33. Pizarro-Cerda J, Charbit A, Enninga J, Lafont F, Cossart P. Manipulation of host
977 membranes by the bacterial pathogens Listeria, Francisella, Shigella and Yersinia. Semin
978 Cell Dev Biol. 2016.
979 34. Lindgren H, Golovliov I, Baranov V, Ernst RK, Telepnev M, Sjostedt A. Factors
980 affecting the escape of Francisella tularensis from the phagolysosome. J Med Microbiol.
981 2004;53(Pt 10):953-8.
982 35. Nano FE, Zhang N, Cowley SC, Klose KE, Cheung KK, Roberts MJ, et al. A
983 Francisella tularensis pathogenicity island required for intramacrophage growth. J Bacteriol.
984 2004;186(19):6430-6.
985 36. Lauriano CM, Barker JR, Yoon SS, Nano FE, Arulanandam BP, Hassett DJ, et al.
986 MglA regulates transcription of virulence factors necessary for Francisella tularensis
987 intraamoebae and intramacrophage survival. Proc Natl Acad Sci U S A. 2004;101(12):4246-
988 9.
989 37. Nano FE, Schmerk C. The Francisella pathogenicity island. Ann N Y Acad Sci.
990 2007;1105:122-37.
991 38. Broms JE, Sjostedt A, Lavander M. The Role of the Francisella Tularensis
992 Pathogenicity Island in Type VI Secretion, Intracellular Survival, and Modulation of Host Cell
993 Signaling. Front Microbiol. 2010;1:136.

994 39. Meibom KL, Dubail I, Dupuis M, Barel M, Lenco J, Stulik J, et al. The heat-shock
995 protein ClpB of Francisella tularensis is involved in stress tolerance and is required for
996 multiplication in target organs of infected mice. Mol Microbiol. 2008;67(6):1384-401.
997 40. Vettiger A, Basler M. Type VI Secretion System Substrates Are Transferred and
998 Reused among Sister Cells. Cell. 2016;167(1):99-110 e12.
999 41. Bröms JE, Sjöstedt A, Lavander M. The Role of the Francisella Tularensis
1000 Pathogenicity Island in Type VI Secretion, Intracellular Survival, and Modulation of Host Cell
1001 Signaling. Front Microbiol. 2010;1:136.
1002 42. Rigard M, Broms JE, Mosnier A, Hologne M, Martin A, Lindgren L, et al. Francisella
1003 tularensis IglG Belongs to a Novel Family of PAAR-Like T6SS Proteins and Harbors a
1004 Unique N-terminal Extension Required for Virulence. PLoS Pathog. 2016;12(9):e1005821.
1005 43. Weiss DS, Brotcke A, Henry T, Margolis JJ, Chan K, Monack DM. In vivo negative
1006 selection screen identifies genes required for Francisella virulence. Proc Natl Acad Sci U S
1007 A. 2007;104(14):6037-42.
1008 44. Broms JE, Lavander M, Sjostedt A. A conserved alpha-helix essential for a type VI
1009 secretion-like system of Francisella tularensis. J Bacteriol. 2009;191(8):2431-46.
1010 45. Spidlova P, Stulik J. Francisella tularensis type VI secretion system comes of age.
1011 Virulence. 2017;8(6):628-31.
1012 46. Ramond E, Gesbert G, Guerrera IC, Chhuon C, Dupuis M, Rigard M, et al.
1013 Importance of host cell arginine uptake in Francisella phagosomal escape and ribosomal
1014 protein amounts. Mol Cell Proteomics. 2015;14(4):870-81.
1015 47. Henry T, Brotcke A, Weiss DS, Thompson LJ, Monack DM. Type I interferon signaling
1016 is required for activation of the inflammasome during Francisella infection. J Exp Med.
1017 2007;204(5):987-94.
1018 48. Jones JW, Kayagaki N, Broz P, Henry T, Newton K, O'Rourke K, et al. Absent in
1019 melanoma 2 is required for innate immune recognition of Francisella tularensis. Proc Natl
1020 Acad Sci U S A. 2010;107(21):9771-6.

1021 49. Meunier E, Wallet P, Dreier RF, Costanzo S, Anton L, Ruhl S, et al. Guanylate-
1022 binding proteins promote activation of the AIM2 inflammasome during infection with
1023 Francisella novicida. Nat Immunol. 2015;16(5):476-84.
1024 50. Jiang Z, Georgel P, Du X, Shamel L, Sovath S, Mudd S, et al. CD14 is required for
1025 MyD88-independent LPS signaling. Nat Immunol. 2005;6(6):565-70.
1026 51. Vettiger A, Winter J, Lin L, Basler M. The type VI secretion system sheath assembles
1027 at the end distal from the membrane anchor. Nat Commun. 2017;8:16088.
1028 52. Salih O, He S, Planamente S, Stach L, MacDonald JT, Manoli E, et al. Atomic
1029 Structure of Type VI Contractile Sheath from Pseudomonas aeruginosa. Structure.
1030 2018;26(2):329-36 e3.
1031 53. Wehrly TD, Chong A, Virtaneva K, Sturdevant DE, Child R, Edwards JA, et al.
1032 Intracellular biology and virulence determinants of Francisella tularensis revealed by
1033 transcriptional profiling inside macrophages. Cell Microbiol. 2009;11(7):1128-50.
1034 54. Meyer L, Broms JE, Liu X, Rottenberg ME, Sjostedt A. Microinjection of Francisella
1035 tularensis and Listeria monocytogenes reveals the importance of bacterial and host factors
1036 for successful replication. Infect Immun. 2015;83(8):3233-42.
1037 55. Ludu JS, de Bruin OM, Duplantis BN, Schmerk CL, Chou AY, Elkins KL, et al. The
1038 Francisella pathogenicity island protein PdpD is required for full virulence and associates
1039 with homologues of the type VI secretion system. J Bacteriol. 2008;190(13):4584-95.
1040 56. Grangeasse C, Nessler S, Mijakovic I. Bacterial tyrosine kinases: evolution, biological
1041 function and structural insights. Philos Trans R Soc Lond B Biol Sci. 2012;367(1602):2640-
1042 55.
1043 57. Brelle S, Baronian G, Huc-Brandt S, Zaki LG, Cohen-Gonsaud M, Bischoff M, et al.
1044 Phosphorylation-mediated regulation of the Staphylococcus aureus secreted tyrosine
1045 phosphatase PtpA. Biochem Biophys Res Commun. 2016;469(3):619-25.
1046 58. Pereira SF, Goss L, Dworkin J. Eukaryote-like serine/threonine kinases and
1047 phosphatases in bacteria. Microbiol Mol Biol Rev. 2011;75(1):192-212.

1048 59. Vincent C, Duclos B, Grangeasse C, Vaganay E, Riberty M, Cozzone AJ, et al.
1049 Relationship between exopolysaccharide production and protein-tyrosine phosphorylation in
1050 gram-negative bacteria. J Mol Biol. 2000;304(3):311-21.
1051 60. Gallagher LA, Ramage E, Jacobs MA, Kaul R, Brittnacher M, Manoil C. A
1052 comprehensive transposon mutant library of Francisella novicida, a bioweapon surrogate.
1053 Proc Natl Acad Sci U S A. 2007;104(3):1009-14.
1054 61. Hunter T. The genesis of tyrosine phosphorylation. Cold Spring Harb Perspect Biol.
1055 2014;6(5):a020644.
1056 62. Chamberlain RE. Evaluation of Live Tularemia Vaccine Prepared in a Chemically
1057 Defined Medium. Appl Microbiol. 1965;13:232-5.
1058 63. Gesbert G, Ramond E, Rigard M, Frapy E, Dupuis M, Dubail I, et al. Asparagine
1059 assimilation is critical for intracellular replication and dissemination of Francisella. Cell
1060 Microbiol. 2014;16(3):434-49.
1061 64. Gesbert G, Ramond E, Tros F, Dairou J, Frapy E, Barel M, et al. Importance of
1062 branched-chain amino acid utilization in Francisella intracellular adaptation. Infect Immun.
1063 2015;83(1):173-83.
1064 65. Klionsky DJ, Abdelmohsen K, Abe A, Abedin MJ, Abeliovich H, Acevedo Arozena A,
1065 et al. Guidelines for the use and interpretation of assays for monitoring autophagy (3rd
1066 edition). Autophagy. 2016;12(1):1-222.
1067 66. Ziveri J, Tros F, Guerrera IC, Chhuon C, Audry M, Dupuis M, et al. The metabolic
1068 enzyme fructose-1,6-bisphosphate aldolase acts as a transcriptional regulator in pathogenic
1069 Francisella. Nat Commun. 2017;8(1):853.
1070 67. Lipecka J, Chhuon C, Bourderioux M, Bessard MA, van Endert P, Edelman A, et al.
1071 Sensitivity of mass spectrometry analysis depends on the shape of the filtration unit used for
1072 filter aided sample preparation (FASP). Proteomics. 2016;16(13):1852-7.
1073 68. Cox J, Mann M. MaxQuant enables high peptide identification rates, individualized
1074 p.p.b.-range mass accuracies and proteome-wide protein quantification. Nat Biotechnol.
1075 2008;26(12):1367-72.

1076 69. Brotcke A, Weiss DS, Kim CC, Chain P, Malfatti S, Garcia E, et al. Identification of
1077 MglA-regulated genes reveals novel virulence factors in Francisella tularensis. Infect Immun.
1078 2006;74(12):6642-55.
1079 70. Coordinators NR. Database Resources of the National Center for Biotechnology
1080 Information. Nucleic acids research. 2017;45(D1):D12-D7.
1081 71. Edgar RC. MUSCLE: multiple sequence alignment with high accuracy and high
1082 throughput. Nucleic acids research. 2004;32(5):1792-7.
1083 72. Fu L, Niu B, Zhu Z, Wu S, Li W. CD-HIT: accelerated for clustering the next-
1084 generation sequencing data. Bioinformatics. 2012;28(23):3150-2.
1085 73. Robert X, Gouet P. Deciphering key features in protein structures with the new
1086 ENDscript server. Nucleic acids research. 2014;42(Web Server issue):W320-4.
1087 74. Vizcaino JA, Csordas A, Del-Toro N, Dianes JA, Griss J, Lavidas I, et al. 2016 update
1088 of the PRIDE database and its related tools. Nucleic Acids Res. 2016;44(22):11033.
1089
1090

1091 Supporting Information Legends

1092

1093 **S1 Fig. Schematic representation of the FPI locus and overview of the T6SS**
1094 **structure of *Francisella.*** The *Francisella* FPI locus representation (*anmK* to *pdpA* gene)
1095 with nomenclature of the canonical T6SS and the *F. novicida* T6SS. A color was assigned for
1096 each gene function and applied on the overview of the T6SS structure.
1097 Red/Green/Blue/Orange, structural protein; Grey, secreted protein; White, hypothetical
1098 protein

1099

1100 **S2 Fig. Alignments of orthologous IglBs proteins.** (**A**) Alignments of orthologous
1101 IglBs proteins showing conservation of Y139 in *Francisellae*. The IglB sequences retrieved
1102 from 19 *Francisella* genomes were aligned using MUSCLE [71] and rendered using ESPript3.0

1103 [73]. Secondary structure elements information is extracted from 3J9O PDB file [32] and is
1104 displayed at the top of the alignment. Sequences are identified by corresponding species
1105 name followed by strain name and locus tag. Species names are abbreviated as follow: Fn,
1106 *Francisella tularensis* subsp. *novicida*; Ftm, *Francisella tularensis* subsp. *mediasiatica*; Fth,
1107 *Francisella tularensis* subsp. *holarctica*; Ftt, *Francisella tularensis* subsp. *tularensis*; Ft,
1108 *Francisella tularensis*; Fno, *Francisella noatunensis*; Fsp, *Francisella* sp. (**B**) Alignments of
1109 orthologous IglBs in other genera showing conservation of a tyrosine residue. Sequences of
1110 11 representative IglB orthologs with a tyrosine residue in the vicinity of Y139 were aligned
1111 using MUSCLE [71] and rendered using ESPript3.0 [73]. Secondary structure elements
1112 information is extracted from 3J9O PDB file [32] and is displayed at the top of the alignment.
1113 Sequences are identified by corresponding Uniprot accession number. Species names are
1114 abbreviated as follow: FRATN, *Francisella tularensis subsp. novicida*; SALTY, *Salmonella*
1115 Typhimurium; YERPE, *Yersinia pestis; BURMA, Burkholderia mallei; XANC5, Xanthomonas*
1116 *campestris; RALP1, Ralstonia pickettii; PHOAA, Photorhabdus asymbiotica; ERWAC,*
1117 *Erwinia amylovora; ENTCC, Enterobacter cloacae; BRAJP, Bradyrhizobium japonicum;*
1118 *RHIFR, Rhizobium fredii; 9GAMM, Serratia nematodiphila.*

1119

1120 **S3 Fig. Effect of IglB mutations on growth in broth.** Wild-type *F. novicida* (WT, Grey
1121 squares), isogenic Δ*iglB* mutant (Δ*iglB*, blue triangles), and complemented *iglB* strain (Cp-
1122 WT, grey circles; Y139A, purple square; Y139F, red square), were grown in Schaedler K3
1123 (left panel) or in Tryptic Soy broth (TSB) supplemented with 0,2% cysteine (right panel).

1124

1125 **S4 Fig. Impact of substitution of Tyr139 by phosphomimetics (Glu or Asp) on**
1126 ***Francisella* intracellular multiplication and T6SS assembly.** (**A**) J774.1
1127 macrophage-like cells were infected in DMEM with 100 MOI of wild-type *F. novicida* (WT)
1128 and mutated strains (Y139E, Y139D, Δ*FPI*) for 24 h. Results are shown as the average of

1129 log_{10} cfu mL^{-1} ± standard deviation. Each experiment was performed in triplicate. **, *p*<0.001
1130 (as determined by two-tailed unpaired Student's *t*-test). (**B**) WB with anti-IglB of sucrose
1131 gradient fractions.

1132

1133 **S5 Fig. Impact of *ptpA* inactivation on *Francisella* intracellular multiplication**
1134 **and T6SS assembly.** (**A**) J774.1 macrophage-like cells were infected in DMEM with 100
1135 MOI of wild-type *F. novicida* (WT), Δ*iglB* mutant, Δ*ptpA* mutant and Δ*FPI* mutant, for 24 h.
1136 Results are shown as the average of log10 cfu mL^{-1} ± standard deviation. Each experiment
1137 was performed in triplicate. **, *p*<0.001 (as determined by two-tailed unpaired Student's *t*-
1138 test). (**B**) Alignments of orthologous PtpAs proteins from different species (FTN, *Francisella*
1139 novicida; Wtb, *Mycobacterium tuberculosis*; *Sau*, *Staphylococcus aureus*). The PtpAs
1140 sequences were aligned using CLUSTALW. (**C**) WBs on bacteria / culture filtrates. Bacteria
1141 were grown in Schaedler-K3 supplemented with 5% KCl until late log phase and then
1142 harvested by centrifugation. Culture supernatants were collected after filtration on 0.2 µM
1143 Millipore filters and concentrated on Amicon 3 kDa. The equivalent of 200 µg of total protein
1144 were loaded onto each well. Left gel, WB with anti-IglC for the culture pellets; right gel, WB
1145 with anti-IglC for the culture supernatants. (**D**) WB with anti-IglB of sucrose gradient fractions.

1146

1147 **S1 Table. Detailed list of phosphosites identified in *F. novicida.*** In this table, we
1148 report: i) the average of the log2 (intensity) of the phosphosites identified from three
1149 independent replicates; ii) the amino acid carrying the phosphorylation ("Amino Acid"); iii) its
1150 position on the protein (Position); iv) the "localization probability" of the phosphosite (1 being
1151 100%); v) the number of replicates the phosphosite has been identified in ("identified"); vi)
1152 the "sequence window" of 15 amino acids before and after the amino acid phosphorylated;
1153 vii) the probability and score of identification and localization (PEP, score, score for

1154 localization); viii) the "charge" of the peptide; and ix) the annotation according to COG and
1155 EggNOG.
1156
1157 **S2 Table 2. Table of intensities for IglB peptide carrying Y139 phosphorylation.**
1158
1159 **S3 Table. List of proteins identified in the "Heavy" (H) and "Light" (L) Fraction**
1160 **in WT and in the Y139F mutant.** WT_H, WT_L, Y139_H, Y139F_L report the log2
1161 (intensity) of the proteins identified in the fractions. Peptides and sequence coverage
1162 indicates the number of total peptides identified and the primary sequence coverage for that
1163 protein across samples. The Q value and the score refer to the quality of the identification.
1164
1165 **S4 Table. Impact of amino acid substitutions at site 139 of IglB on sheath**
1166 **assembly.**
1167
1168 **S5 Table. Strains and plasmids.**
1169
1170
1171

A

Y
T
S
82
p-sites

B

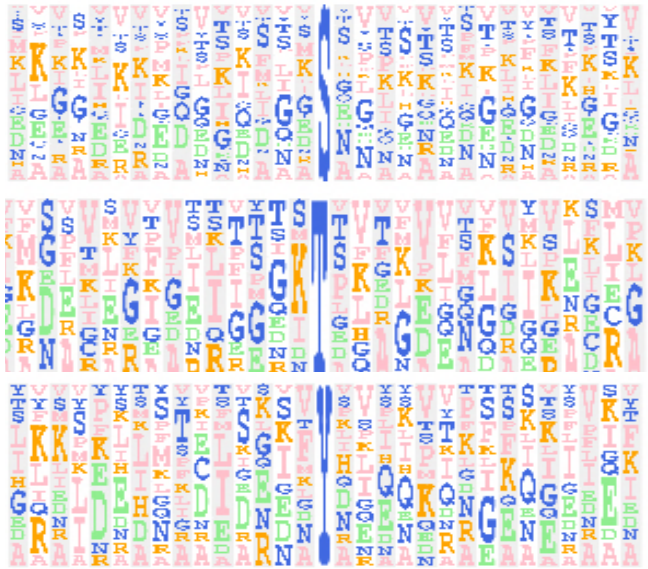

C

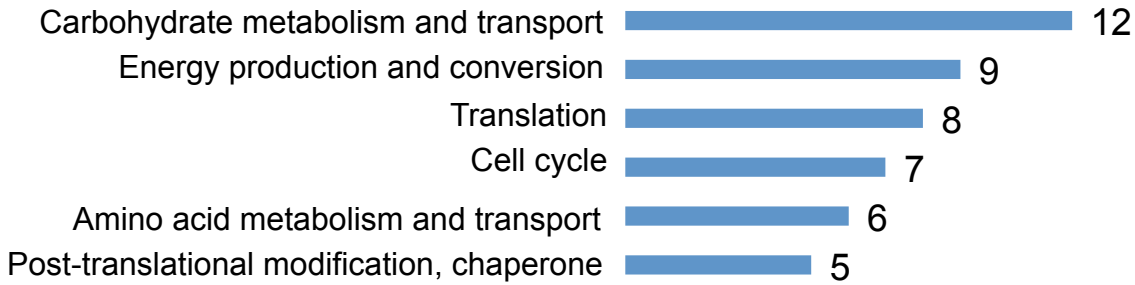
Carbohydrate metabolism and transport
12
Energy production and conversion
9
Translation
8
Cell cycle
7
Amino acid metabolism and transport
6
Post-translational modification, chaperone
5

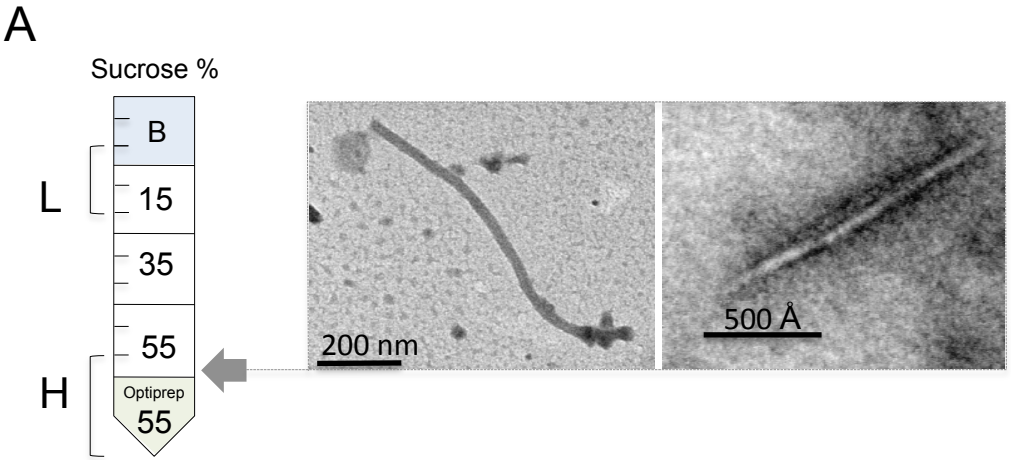
A
Sucrose %
B
L
15
35
55
H
Optiprep
55
200 nm
500 Å

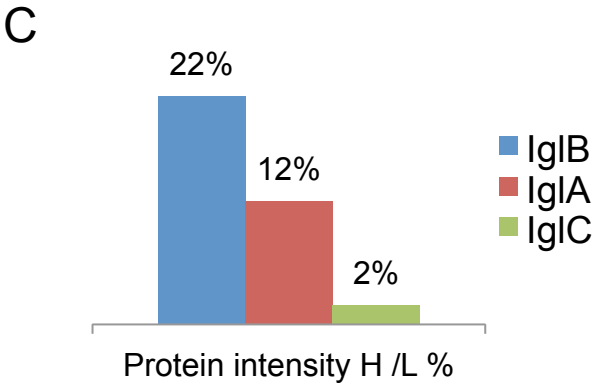
C
22%
12%
2%
IglB
IglA
IglC
Protein intensity H /L %

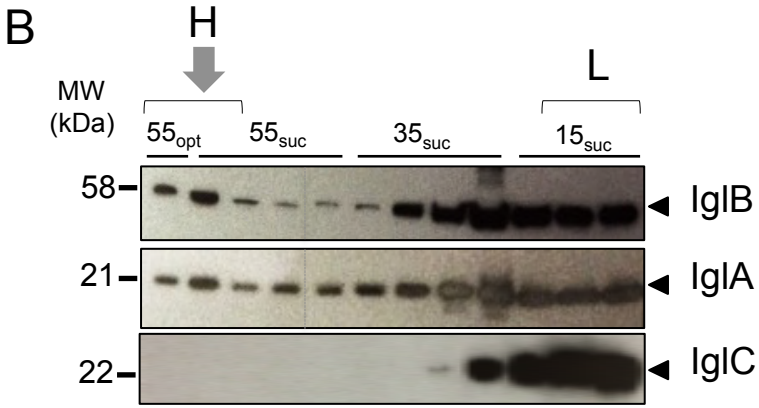
B
H
L
MW
(kDa)
55opt
55suc
35suc
15suc
58
21
22
IglB
IglA
IglC

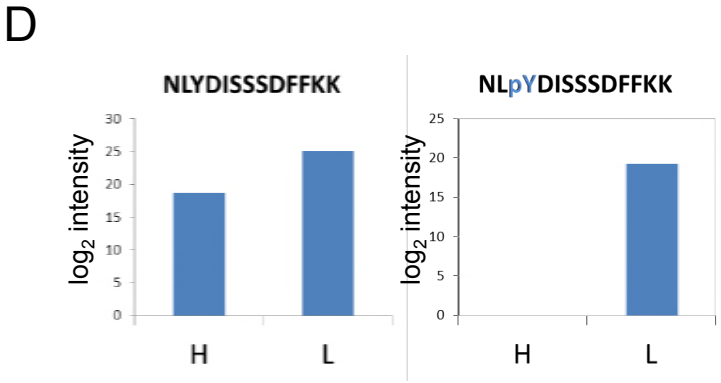
D
NLYDISSSDFFKK
NLpYDISSSDFFKK
log2 intensity
30
25
20
15
10
5
0
H
L

A

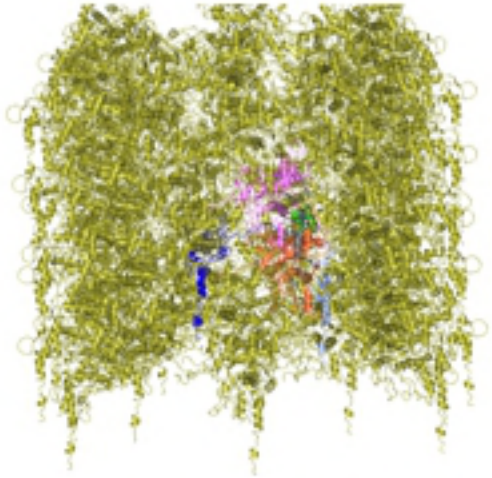

B

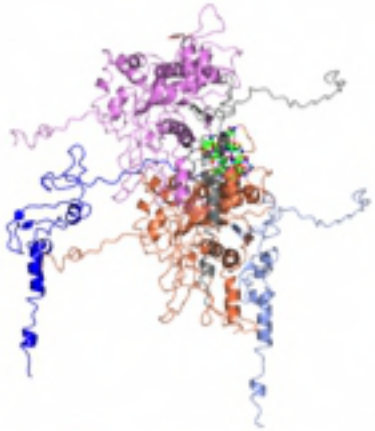

C

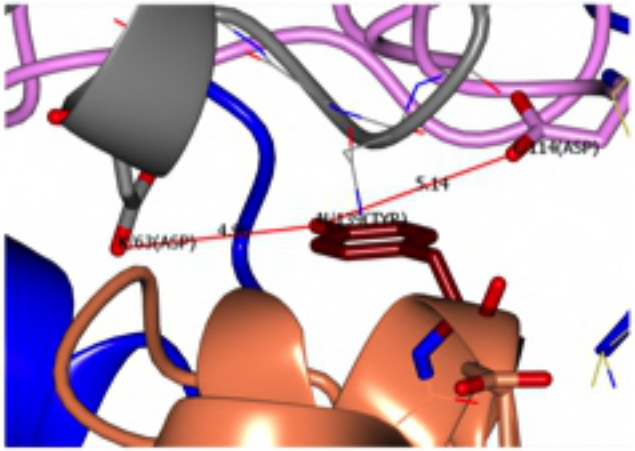

D

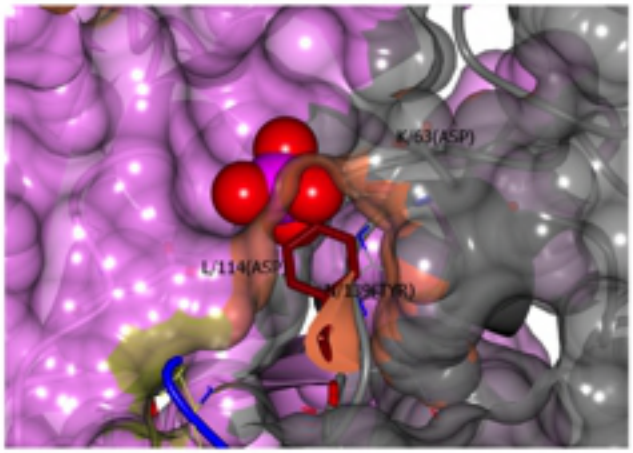

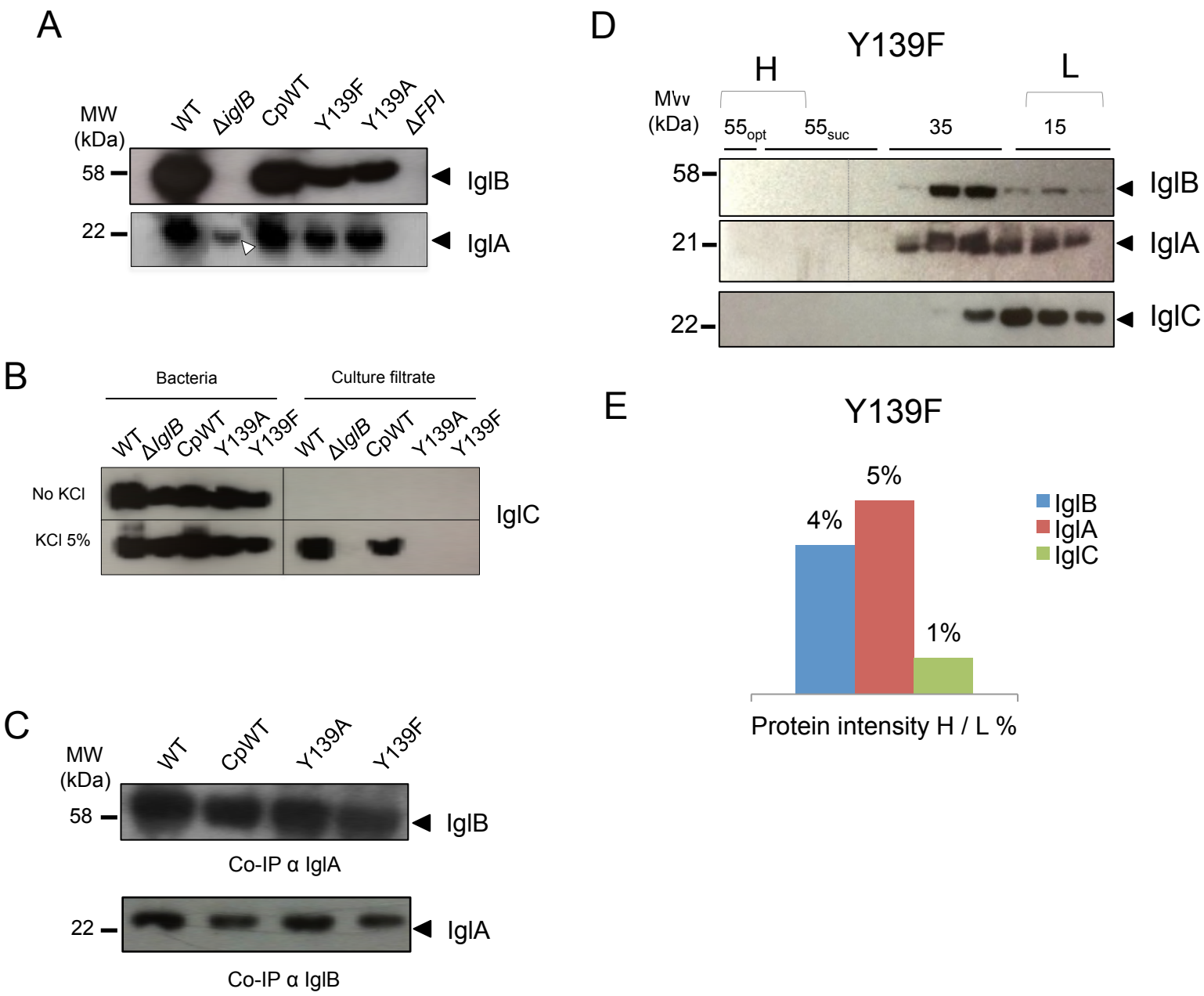
A
MW (kDa)
WT
ΔiglB
CpWT
Y139F
Y139A
ΔFPI
58
22
IglB
IglA
B
Bacteria
Culture filtrate
WT
ΔiglB
CpWT
Y139A
Y139F
WT
ΔiglB
CpWT
Y139A
Y139F
No KCl
KCl 5%
IglC
C
MW (kDa)
WT
CpWT
Y139A
Y139F
58
IglB
Co-IP α IglA
22
IglA
Co-IP α IglB
D
Y139F
H
L
Mvv (kDa)
55opt
55suc
35
15
58
21
22
IglB
IglA
IglC
E
Y139F
5%
4%
1%
IglB
IglA
IglC
Protein intensity H / L %

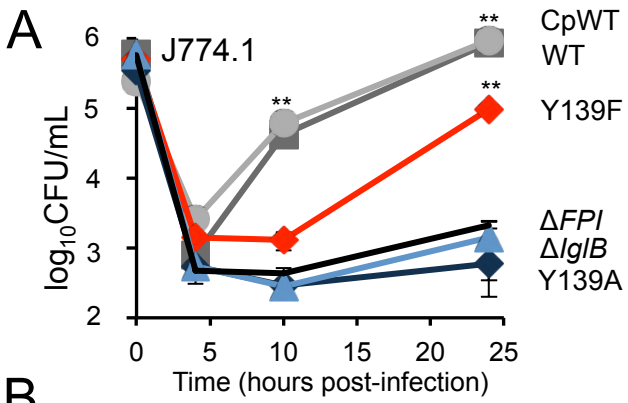
A
J774.1
log10CFU/mL
Time (hours post-infection)
CpWT
WT
Y139F
ΔFPI
ΔIglB
Y139A
**

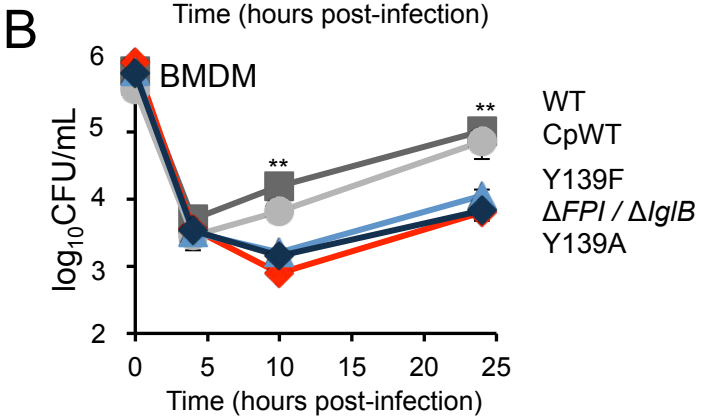
B
BMDM
log10CFU/mL
Time (hours post-infection)
WT
CpWT
Y139F
ΔFPI / ΔIglB
Y139A
**

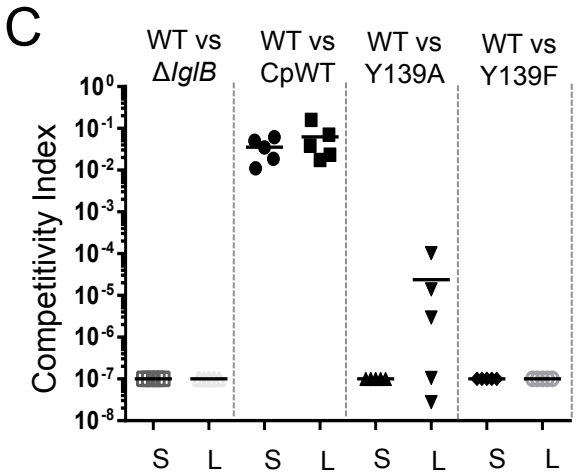
C
WT vs ΔIglB
WT vs CpWT
WT vs Y139A
WT vs Y139F
Competitivity Index
S
L

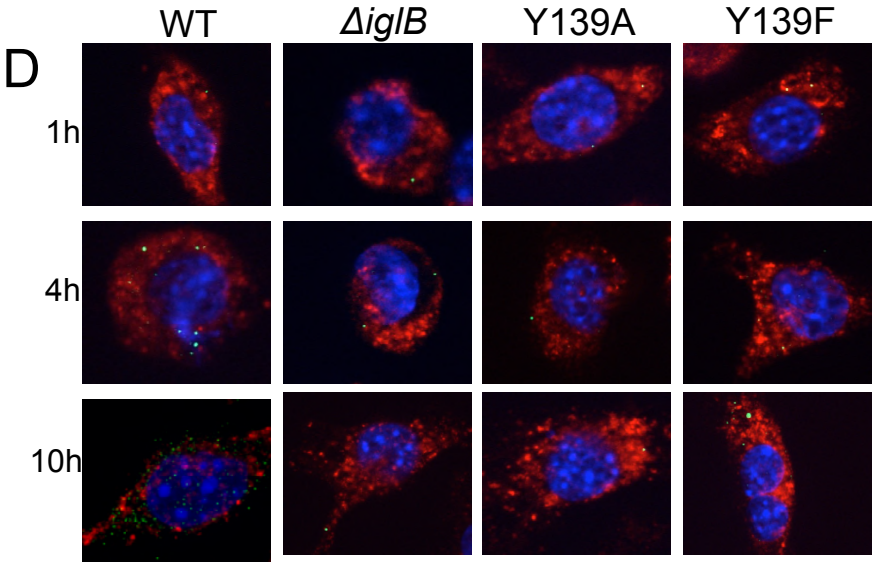
D
WT
ΔiglB
Y139A
Y139F
1h
4h
10h

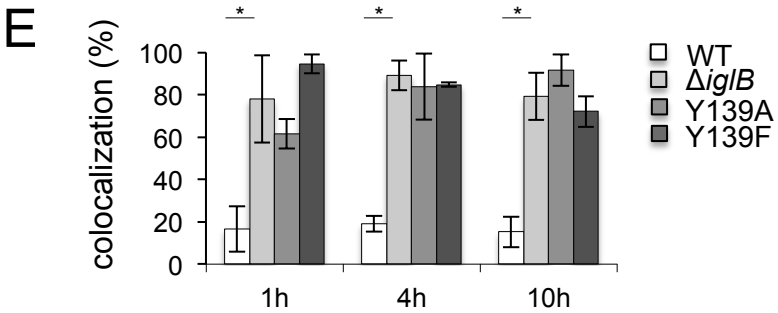
E
colocalization (%)
1h
4h
10h
WT
ΔiglB
Y139A
Y139F

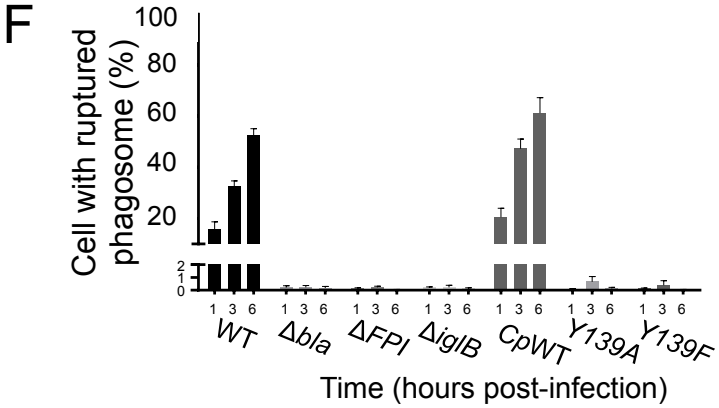
F
Cell with ruptured phagosome (%)
WT
Δbla
ΔFPI
ΔiglB
CpWT
Y139A
Y139F
Time (hours post-infection)

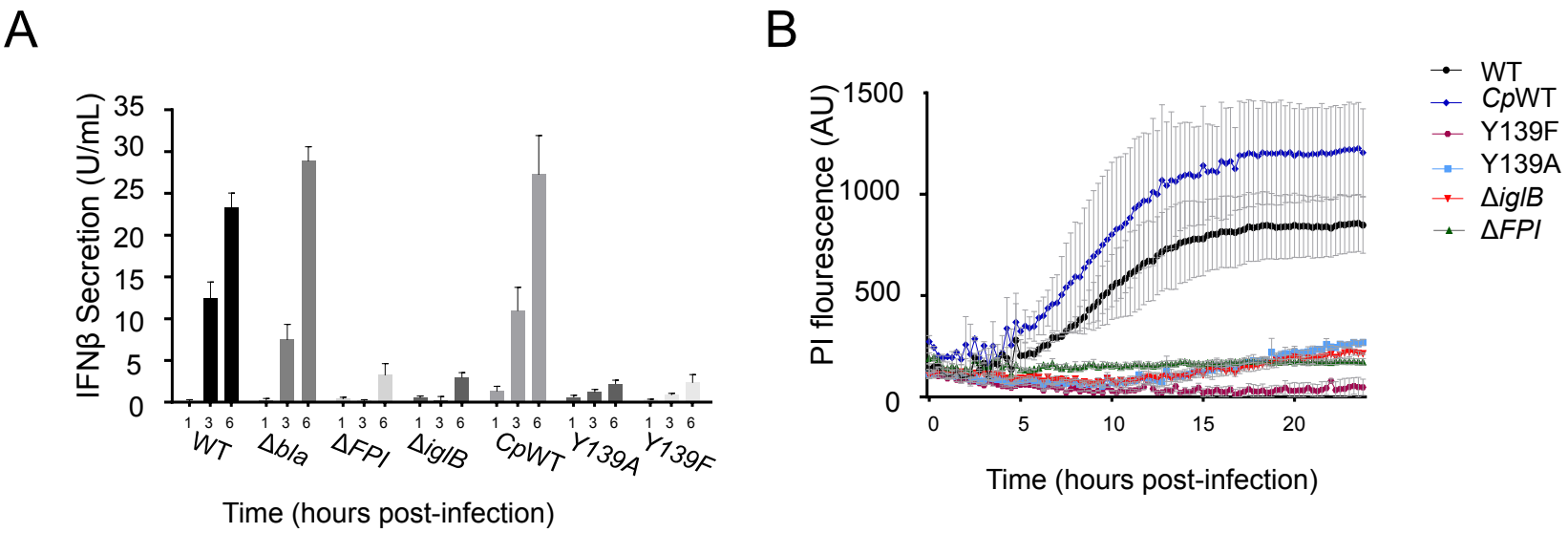
A
IFNβ Secretion (U/mL)
35
30
25
20
15
10
5
0
1 3 6
WT
Δbla
ΔFPI
ΔiglB
CpWT
Y139A
Y139F
Time (hours post-infection)
B
PI flourescence (AU)
1500
1000
500
0
0
5
10
15
20
Time (hours post-infection)
WT
CpWT
Y139F
Y139A
ΔiglB
ΔFPI

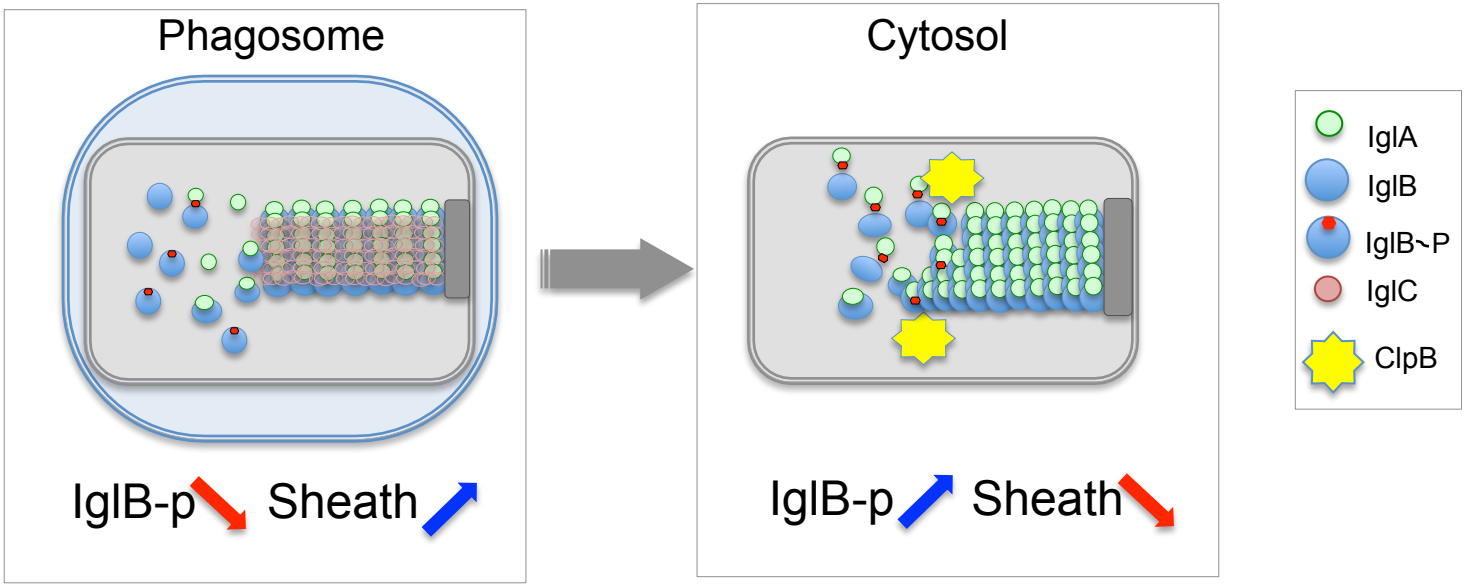
Phagosome
IglB-p
Sheath
Cytosol
IglB-p
Sheath
IglA
IglB
IglB~P
IglC
ClpB